

# Low-Dimensional Semiconductor Superlattices Formed by Geometric Control over Nanocrystal Attachment

Wiel H. Evers,<sup>†</sup> Bart Goris,<sup>‡</sup> Sara Bals,<sup>‡</sup> Marianna Casavola,<sup>†</sup> Joost de Graaf,<sup>§</sup> René van Roij,<sup>||</sup> Marjolein Dijkstra,<sup>§</sup> and Daniël Vanmaekelbergh<sup>\*,†</sup>

<sup>†</sup>Condensed Matter and Interfaces, Debye Institute for Nanomaterials Science, Utrecht University, Princetonplein 1, P.O. Box 80.000, 3508 TA, Utrecht, The Netherlands

<sup>‡</sup>EMAT, Department of Physics, University of Antwerpen, Groenenborgerlaan 171, 2010 Antwerpen, Belgium

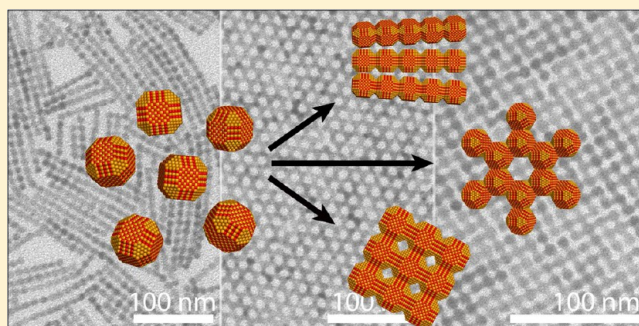
<sup>§</sup>Soft Condensed Matter, Debye Institute for Nanomaterials Science, Utrecht University, Princetonplein 1, P.O. Box 80.000, 3508 TA, Utrecht, The Netherlands

<sup>||</sup>Institute for Theoretical Physics, Utrecht University, Leuvenlaan 4, P.O. Box 80.000, 3508 TA, Utrecht, The Netherlands

## S Supporting Information

**ABSTRACT:** Oriented attachment, the process in which nanometer-sized crystals fuse by atomic bonding of specific crystal facets, is expected to be more difficult to control than nanocrystal self-assembly that is driven by entropic factors or weak van der Waals attractions. Here, we present a study of oriented attachment of PbSe nanocrystals that counteract this intuition. The reaction was studied in a thin film of the suspension casted on an immiscible liquid at a given temperature. We report that attachment can be controlled such that it occurs with one type of facets exclusively. By control of the temperature and particle concentration we obtain one- or two-dimensional PbSe single crystals, the latter with a honeycomb or square superimposed periodicity in the nanometer range. We demonstrate the ability to convert these PbSe superstructures into other semiconductor compounds with the preservation of crystallinity and geometry.

**KEYWORDS:** Self-assembly, oriented attachment, nanocrystals, honeycomb, artificial graphene



Oriented attachment, the connection of a nanometer-sized crystal to another crystal via atomic matching of opposing crystal facets, is an intriguing process that is important in crystal growth and biomineralization.<sup>1–3</sup> In bottom-up approaches that aim to produce extended and highly ordered nanostructures using wet chemistry, oriented attachment is increasingly employed to grow highly anisotropic semiconductor nanostructures.<sup>4–9</sup> This is enabled by recent progress to synthesize colloidal nanocrystals with a uniform size and shape and, hence, with well-defined crystal facets. The adsorption–desorption equilibria of the nanocrystal surfactant molecules, which are responsible for the colloidal stability, are specific for different nanocrystal facets.<sup>10–12</sup> This facet-specific surfactant adsorption can play a decisive role in which facet(s) becomes reactive in nanocrystal attachment, determining in this way the geometry of the resulting structures. In this respect, nanocrystals of the lead chalcogenide family have been studied extensively. By adding specific surfactant molecules or cosolvents to the nanocrystal suspension, specific crystallographic facets can be “activated”, resulting in 1-D semiconductor nanowires in some cases and 2-D sheets in other cases. Cho et al. reported the formation of micrometer-long PbSe wires at elevated temperature, formed by the consecutive

attachment of PbSe nanocrystals via their opposite {100} facets.<sup>4</sup> More recently, the formation of ultrathin single crystalline PbS sheets initiated by addition of a Cl-containing cosolvent to the suspension was reported.<sup>7</sup> Since the resulting structures are either 1-D wires or 2-D sheets that are highly crystalline, oriented attachment could become a new approach for the fabrication of 1-D and 2-D semiconductors with importance for nanophysics and opto-electronic applications.

Oriented attachment of colloidal nanocrystals is different from nanocrystal self-assembly in the strength of the driving forces, being interatomic bonding in the first and van der Waals interactions or entropic factors in the second case.<sup>13</sup> It can hence be expected that oriented attachment is an irreversible aggregation process that is more difficult to control by the reaction conditions than by nanocrystal self-assembly. Here we present results that counteract this intuition. We studied the oriented attachment of PbSe nanocrystals in a thin film of a suspension casted on an immiscible liquid at temperatures whereby the solvent evaporates. We show that, by variation of

**Received:** September 6, 2012

**Revised:** October 8, 2012

**Published:** October 11, 2012

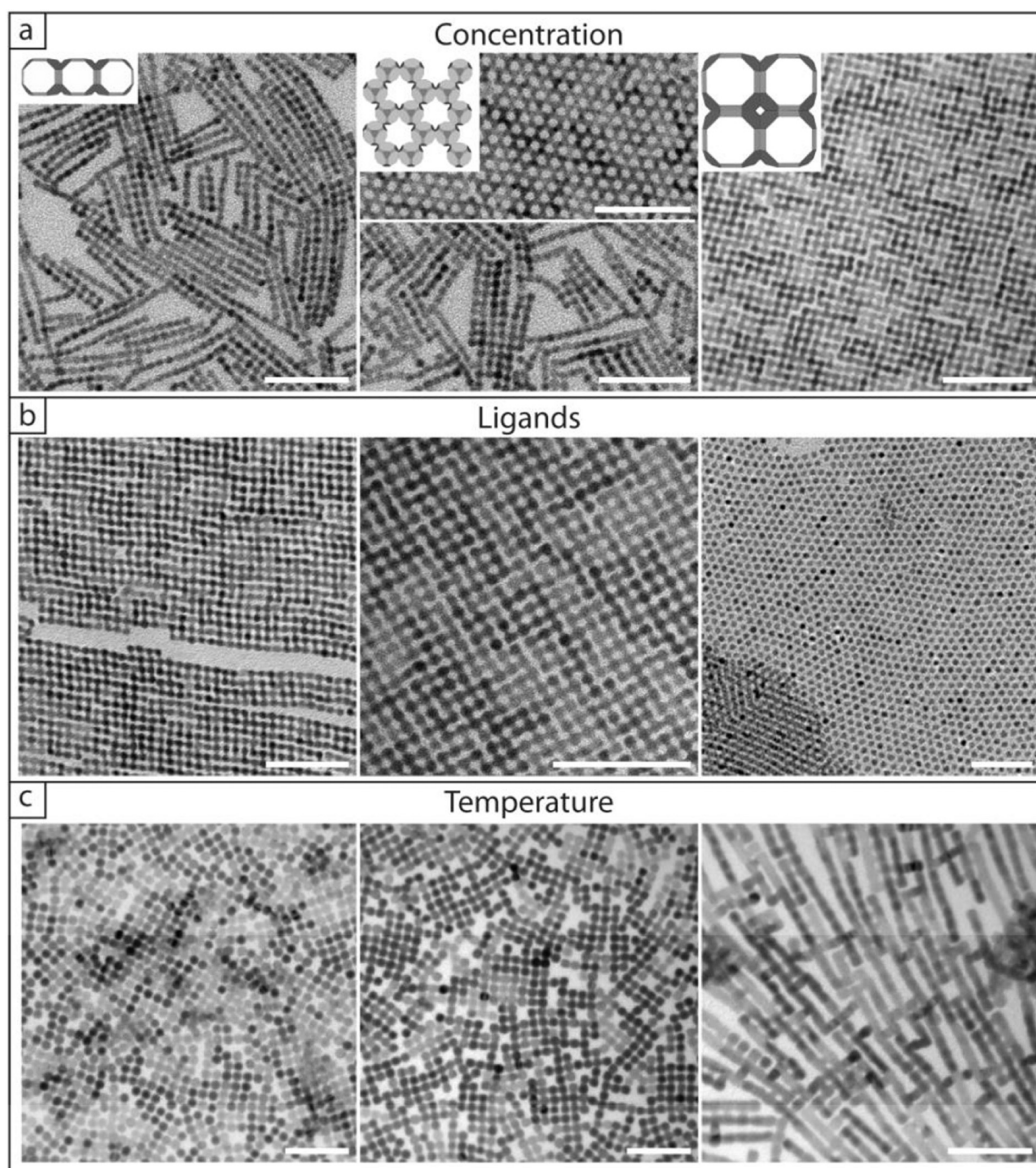


**Figure 1.** Effects of the reaction parameters on the structures formed by oriented attachment of PbSe nanocrystals. The structural characterization was performed by TEM. (a) Effect of the initial particle concentration in the NC suspension. The colloidal building blocks were truncated PbSe cubes with a size of 5.4 nm capped with oleic acid; the reaction temperature was 50 °C. The initial particle concentrations are: left,  $7.0 \times 10^{-7}$ ; center,  $11.3 \times 10^{-7}$ ; right,  $28 \times 10^{-7}$  mol/L. No additional capping ligands were added to the ethylene glycol solution. The insets show cartoons of the linear structures, honeycomb superlattices, and ultrathin sheets with square nanostructuring. (b) Effect of oleic acid ligand addition to the ethylene glycol liquid substrate. The building blocks were truncated PbSe cubes with a size of 5.4 nm capped with oleic acid; the reaction temperature was 50 °C, and the initial particle concentration was  $28 \times 10^{-7}$  mol/L. The concentrations of added oleic acid in the ethylene glycol are: left; no additional ligands added, center:  $4 \times 10^{-5}$  mol/L, right:  $4 \times 10^{-4}$  mol/L. (c) Effect of reaction temperature. The building blocks were truncated PbSe cubes with a size of 7.5 nm capped with oleic acid; the initial particle concentration in the suspension was  $14 \times 10^{-7}$  mol/L. The reaction temperature was left: 45, center: 100, and right: 140 °C. All scale bars represent 50 nm. No additional capping ligands were added to the ethylene glycol solution.

the nanocrystal concentration and the temperature, the symmetry of attachment can be varied from linear to two-dimensional and even to three-dimensional. In the two-dimensional case we are able to prepare ultrathin sheets with a square and honeycomb superlattice structure. The resulting structures are suspended on the immiscible substrate liquid and can thus be transferred to any substrate of choice, which enables their incorporation in opto-electronic devices. Moreover, we demonstrate the ability to convert these rods and sheets to other compounds such as CdSe and  $\text{Cu}_{2-x}\text{Se}$ , opening

the pathway to two-dimensional superlattices of a variety of semiconductor compounds.

We used suspensions of truncated PbSe nanocubes, nanorods, and stars that were nearly uniform in size and shape; high angle annular dark field scanning electron transmission (HAADF-STEM) pictures that present the crystal shapes are given in the Supporting Information (SI). The PbSe nanocubes employed are truncated and appear consistent with a model with 6 {100} initial planes, 12 {110} planes, and 8 {111} planes, and the sizes are varied between 4 and 10 nm. A model is presented in the SI, theoretical section. Typically, 50  $\mu\text{L}$  of

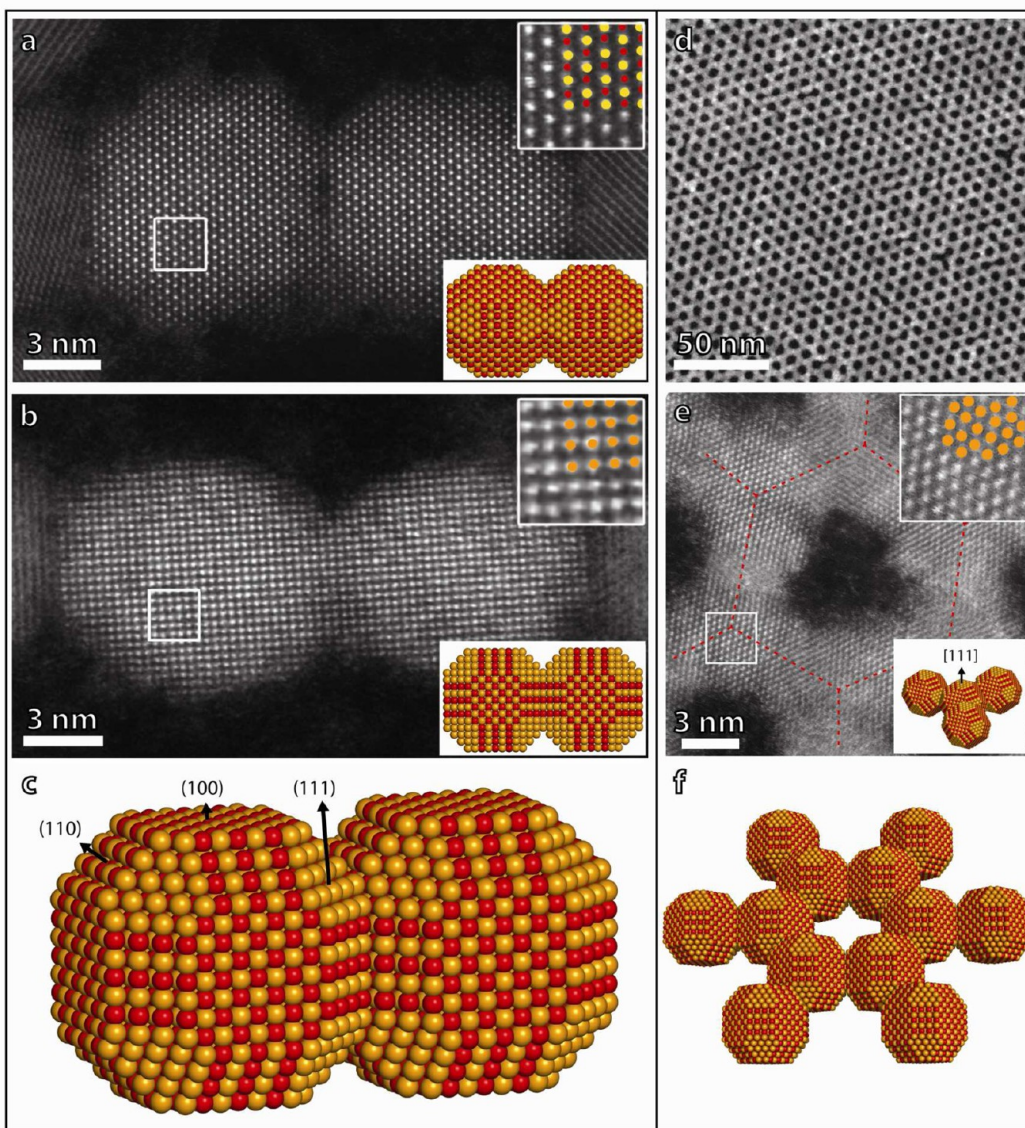


**Figure 2.** Atomic details of the oriented attachment of PbSe nanocrystals as revealed by HAADF-STEM. Left panel: oriented attachment via  $\{100\}$  facets leading to wires or ultrathin sheets. (a) HAADF-STEM image of two fusing NCs along the  $[110]$  projection. (b) HAADF-STEM image of two fusing NCs along the  $[100]$  projection. In the inset of a and b, a detailed zoom is given with atomic overlay of the atomic columns (yellow Pb, red Se, orange Pb and Se). The PbSe NCs are attached along the  $\{100\}$  facets. (c) Model of the two fused NCs. Right panel: Oriented attachment via the  $\{110\}$  facets resulting in a honeycomb superlattice. (d) Overview of the honeycomb lattice; (e) detailed HAADF-STEM picture showing the  $[111]$  projection of the original building blocks; (f) 3-dimensional model with atomic resolution showing how the building blocks are attached via the  $\{110\}$  facets.

the suspension was placed on ethylene glycol, being a nearly immiscible liquid for the suspension. The solvent of the suspension was evaporated under a nitrogen atmosphere at a given reaction temperature. The only three parameters that we varied were (i) the initial nanocrystal concentration in the suspension, (ii) the temperature at which the solvent was evaporated, and (iii) the concentration of oleic acid capping molecules that we added into the ethylene glycol substrate liquid. Further details are presented in the SI.

It has been reported that the solvent evaporation in a similar reactor system induces the self-assembly of colloidal nanocrystals into well-ordered and self-supported nanocrystal membranes held together by van der Waals attractions between the capping molecules.<sup>14</sup> In line with this, we observed hexagonally ordered monolayers of PbSe nanocrystals if we used PbSe nanocrystals protected with an inactive CdSe shell

(SI, Figure S4A, central panel). However, when we used the oleic acid capped PbSe nanocrystals, the nanocrystal ordering in the structures formed by solvent evaporation changed dramatically and was accompanied by oriented attachment of the crystals, instead of self-assembly driven by van der Waals attractions.

We first review the effect of the three reaction parameters on the structures obtained by nanocrystal attachment; see Figure 1, panels a, b, and c. More complete data sets are presented in the SI, Figures S4–S7. Figure 1 a shows the effect of the initial nanocrystal concentration for nanocrystals of 5.4 nm in size, for a reaction carried out at a temperature of 50 °C. Notice that, at low particle concentrations, the attachment of the nanocrystals led to disordered aggregates; examples are given in the SI (Figure S4). However, above a given nanoparticle concentration, the attachment led to ordered structures with a well-

defined geometry being determined by the nanoparticle concentration. This means that, under given conditions, only one type of facet is active in the crystal bonding, and that there is a directional control in the nanocrystal attachment. The TEM pictures in Figure 1a show that the crystal attachment resulted in nanocrystal wires, a 2-D honeycomb lattice, and finally a 2-D square lattice by simply increasing the particle concentration. Figures S4 and S6 (SI) present the structures formed by 9.9 nm PbSe cubes treated at 100 °C: rod-like systems were observed at  $\sim 2 \times 10^{-7}$  mol/L, perfect planar sheets with square nanocrystal ordering at  $\sim 11 \times 10^{-7}$  mol/L, and 3-D sheets at particle concentrations larger than  $\sim 21 \times 10^{-7}$  mol/L. We remark that the previously reported formation of linear structures or 2-D sheets by attachment of Pb-chalcogenide nanocrystals demands different crystals (PbSe and PbS) and reaction conditions. Here, however, we show that, in one colloidal system, the particle concentration can control the dimensionality and the nanoscale geometry (2-D honeycomb and 2-D square) of the formed structures.

The findings above suggest that the detachment of the capping molecules from specific facets and dissolution of these in the ethylene glycol drives crystal attachment. To further investigate this, we monitored the effect of addition of capping molecules to the ethylene glycol (Figure 1b and SI, Figures S8 and S9). From the results it becomes clear that the addition of sufficient capping molecules to the ethylene glycol stabilizes all facets of the particles, prevents oriented attachment, and leads to the formation of self-assembled hexagonal (mono) layers of stable particles. This shows that the equilibria involving the capping molecules in the suspension (free and attached to the NC facets) and the glycol phase are of primary importance in the controlled reactions that we observe. In this view, the disordered NC aggregation that we observed at low particle concentration can be understood as being the effect of a very low concentration of free ligands in the suspension and the glycol liquid substrate resulting in the stripping of the capping molecules from different NC facets and random crystal attachment.

The effect of the temperature at a given particle concentration can be followed via the horizontal panels of Figure 1C; more examples are presented in the SI, Figures S4, S5, and S7. At a sufficiently high particle concentration, square 2-D sheets formed at lower temperature (45 °C), whereas at higher temperatures (branched) rods were favored.

The results so far showed that the reaction parameters can control the geometry of the formed structures. With the smaller 5.4 nm PbSe particles, there are even two different planar geometries: the honeycomb superlattice and the square sheet. The striking uniformity of the resulting structures shows that only one type of facet is involved in the reaction under given conditions. The atomic details of crystal attachment were further elucidated by a detailed HAADF-STEM<sup>15</sup> study; see Figure 2 and Figures S10–12 and S14 in the SI. Figure 2 a and b shows typical HAADF-STEM images of the linear attachment of two nanocrystals. The atomic columns of Pb and Se can be observed separately along the [110] viewing axis in Figure 2a. Along the [100] viewing axis (Figure 2b), the atomic columns contain both Pb and Se (see atomic overlays). Panel C shows a 3-D illustrative model of how two cubes attached in a linear fashion. For the PbSe wires and square sheets it was observed that crystal attachment occurred mostly via  $\langle 100 \rangle / \langle 100 \rangle$  connections, while  $\langle 100 \rangle / \langle 110 \rangle$  and  $\langle 110 \rangle / \langle 110 \rangle$  connections, breaking the overall square symmetry, are infrequent.

Anomalous attachments and defects in the structures can be characterized by HAADF-STEM; see SI, Figure S10. It is clear that, in the example presented in Figure 2a–c, the attachment occurred with full atomic matching of the {100} planes. The connection plane contains columns with considerably less atoms, which is directly related to the shape of the truncated nanocubes involved. The XRD patterns of 2-D sheets formed by oriented attachment indicate that the nanocrystals are uniformly oriented with their [100] axis perpendicular to the substrate, in agreement with attachment involving exclusively the four vertical {100} facets. Further evidence for nearly exclusive attachment via {100} planes followed from the use of PbSe nanorods and stars; see SI, Figures S12–S14. HAADF-STEM showed that the nanorods that we used had a smooth {100} facet termination at both tips, while the long sides are {100} facets that were considerably roughened (SI, Figure S3). In this case, attachment resulted in the formation of wires only, formed by linear connection of the rods without 2-D branching. Possibly, the roughness of the {100} facets at the long sides prevents the formation of 2-D structures. The PbSe stars can be seen as cubes with a pyramid grown on each of the {100} facets. These crystals did not display {100} facets, except for presumably small facets at the tip ends. Strikingly, solvent evaporation at increased temperature led to the formation of attached stars displaying a linear or planar square symmetry; the connections occurred only via the sharp tips. This demonstrates the astounding dominance of the {100} facets in the attachment process. In contrast, however, the remarkable honeycomb superlattices cannot be understood by attachment of the {100} facets. The atomic details of the honeycomb superstructures investigated by HAADF-STEM are presented in Figure 2 d–f. It was observed that the nanocrystals are all oriented with the [111] direction perpendicular to the 2-D sheet plane. Using models for truncated nanocubes, it became clear that this specific orientation is the only way to form a honeycomb lattice and that the {110} facets are exclusively involved in atomic bonding. Three of the 12 {110} facets of each nanocrystal are used, as shown in Figure 2e,f. Theoretical work shows that the {100} facets have a somewhat lower surface energy than the {110} facets and much lower in energy than the {111} facets.<sup>16</sup> This suggests that the dominance of the {100} facets in attachment is due to the fact that at this facet the adsorption equilibrium is shifted the most in the direction of free capping molecules in the suspension and the underlying glycol liquid. The higher energy {110} and Pb-terminated {111} facets remain better protected by the oleic acid capping molecules. That such adsorption/desorption equilibria are key for further understanding is shown by the fact that addition of a small amount of capping molecules in the glycol liquid substrate prevents oriented attachment. However, we should remark that the sudden transition from the linear attachment via {100} facets to the honeycomb lattice via {110} facets to the square sheets again via {100} facets is beyond understanding.

The exclusive use of one type of crystal facets, that is, {100} or {110}, together with the control over the dimensions and the nanoscale geometry by the particle concentration and temperature is remarkable and nontrivial. Here, we attempt to present the main factors that will be required for further understanding. The formation of extended low-dimensional PbSe crystals, that is, wires and square sheets from cubic building blocks that have six equivalent {100} facets, must be the result of symmetry breaking. This indicates that oriented

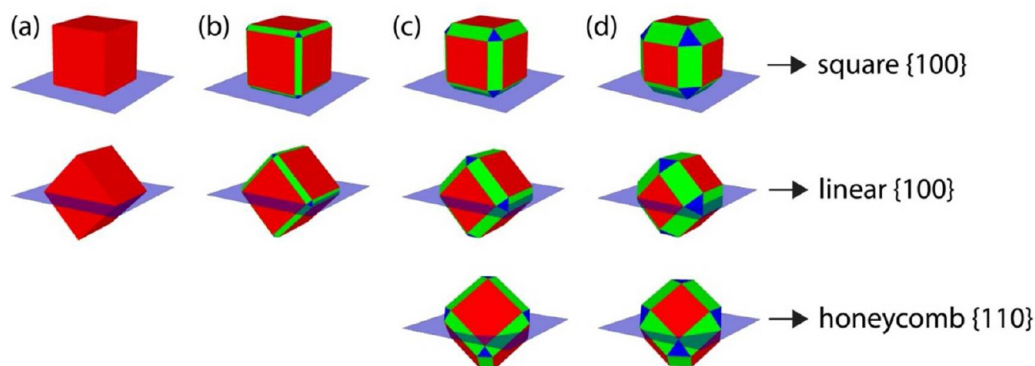


**Figure 3.** Prototypical equilibrium configurations for truncated PbSe nanocubes adsorbed to a flat toluene–air interface as determined by our theoretical approach; also see the SI section. The level of truncation increases from left to right, and the various crystal facets are indicated using three colors: (red)  $\{100\}$  facets, (green)  $\{110\}$  facets, and (blue)  $\{111\}$  facets. The interface is given by a translucent blue square. (a) For a cube we find exactly two possible adsorption equilibria: one with the normal to one of the  $\{100\}$  facets pointing toward the  $z$ -axis and one where the normal to one of the  $\{110\}$  “facets” is pointing upward. (b) For slightly greater levels of truncation we again find these two configurations. (c–d) For even greater levels of truncation a third configuration appears, for which the normal to one of the  $\{111\}$  facets is pointing upward.

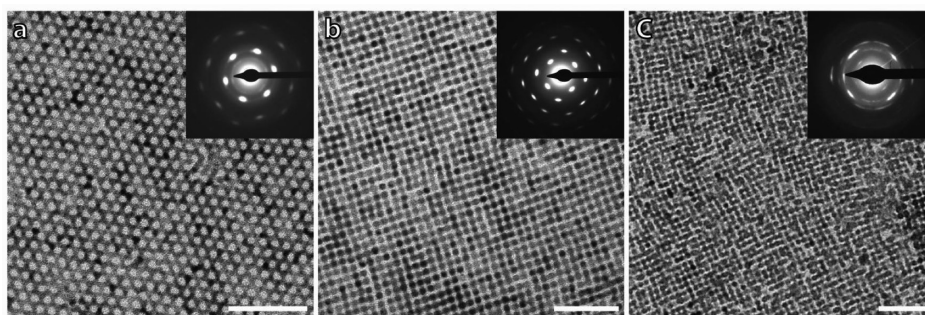


**Figure 4.** Overview of ultrathin nanostructured semiconductor crystals formed by oriented attachment of 5.4 nm PbSe nanocrystals. (a) Ultrathin PbSe rocksalt semiconductor sheet with a honeycomb nanostructuring. The periodicity of the honeycomb structure is 6.5 nm. Inset: electro-diffractogram showing the PbSe rocksalt lattice in the  $[111]$  projection. (b) Ultrathin PbSe rocksalt semiconductor sheet with a square nanostructuring. The periodicity of superlattice structure is 6.6 nm. Inset: electro-diffractogram showing the PbSe rocksalt lattice in the  $[100]$  projection. (c) Ultrathin CdSe semiconductor with a compressed zincblende atomic structure and slightly distorted square nanostructuring. Inset: electro-diffractogram showing the CdSe zincblende lattice in the  $[100]$  projection. All scale bars represent 50 nm.

attachment in our reactor system takes place at an interface. To support this conjecture, we investigated theoretically the adsorption of our cubic nanocrystals at the air–toluene interface. The experimental system was studied using a simple model of a truncated cube adsorbed at a flat *undeformed* interface, for which only surface-tension contributions to the free energy of adsorption were taken into account. Our model is thus in the spirit of the early investigations of colloid adsorption by Pieranski.<sup>17</sup> We analyzed the equilibrium orientation of the nanocrystals at the interface as a function of the surface properties (as described by the contact angle) of the different types of facet:  $\{100\}$ ,  $\{110\}$ , and  $\{111\}$ , which we allowed to vary independently of each other, and as a function of the level of truncation. Remarkably, we found that by varying the contact angles and level of truncation only a limited number of “prototypical” equilibrium adsorption orientations were found. We discuss our findings below and refer to the SI section for further details on the methods used.

We observed that for limited levels of truncation (e.g., for the 9.9 nm PbSe nanocubes) there are two preferred geometries associated to the adsorption, that is, configurations which minimize the free energy. One of the two corresponds to the PbSe nanocube adsorbed at the interface via a  $\{100\}$  facet (Figure 3a,b), while the other one is absorbed via the  $\{110\}$  facet, which implies that respectively the four adjacent or two

opposite  $\{100\}$  facets are standing perpendicular to the interface, leaving these free to be involved in oriented attachment in a square- or rod-like fashion in the direction parallel to the plane of the interface, in the way sketched in Figure 2a–c. Alternatively, Cho et al. argued that linear attachment is mediated by a residual electric dipole resulting from the uneven distribution of the  $\{111\}$  Pb and Se facets; once two nanocrystals are attached, the electrical dipole is enhanced leading to further elongation of the rod by new linear attachment events.<sup>4</sup> It should however be remarked that, according to molecular dynamics simulations, the  $\{111\}$  Se planes are considerably reconstructed, leading to a charge reduction.<sup>18</sup> Another point that needs further attention is the formation of the honeycomb superstructures in which each nanocrystal uses three  $\{110\}$  facets. Our calculations show that attachment of the PbSe nanocubes with a  $[111]$  direction perpendicular to the interface is one of the three possible adsorption configurations (see Figure 3c,d and SI, theoretical section) that minimize the free energy in case the nanocrystals are considerably truncated (as the 5.4 nm nanocubes). In this adsorption configuration, the truncated  $\{110\}$  planes have an angle of  $0.6\pi$  with the interface and are available for oriented attachment in the way sketched in Figure 2e,f, resulting in the honeycomb superstructure. It is, however, not easy to understand why the adsorption geometry changes from

perpendicular [111] to [100] by simply increasing the particle concentration.

The two-step bottom-up method that we present here, that is, the synthesis of well-defined nanocrystals from atomic precursors, followed by oriented attachment under mild conditions in a thin film of suspension casted on an immiscible liquid, holds promise for the fabrication of one and two-dimensional semiconductors with applications in nanophysics and opto-electronic devices.<sup>14,19,20</sup> The work presented above shows that, with PbSe nanocube building blocks, simple reaction parameters such as the temperature and particle concentration can be used to prepare 1-D rods and 2-D nanostructured sheets at will. Moreover, the reaction can be moderated by controlled addition of oleic acid capping molecules to the ethylene glycol substrate. The use of a liquid ethylene glycol substrate has another important asset: the products of oriented attachment are suspended on a liquid substrate and can, in this way, be transferred to a solid substrate or an electrical device or be used in soft printing techniques. Some examples of two-dimensional ultrathin sheets with a honeycomb and square nanostructuring are presented in Figure 4. The electro-diffractograms presented in the insets of Figure 4 a,b show that overall the structures are single crystalline (rocksalt PbSe) with an added superstructure periodicity in the nanometer range. This is in line with HAADF-STEM results displayed in Figure 2 that show smooth atomic connections between the nanocrystals. Recently, there has been much interest in the effects of superperiodicity on the electronic properties of semiconductors and confined two-dimensional electron gases.<sup>21–24</sup> It has, for instance, been shown that, when a two-dimensional fermion gas is subject to a honeycomb periodic potential, this results in the emergence of an electronic sub-band with a linear energy-wave vector relationship, in a similar way as for graphene. A honeycomb nanometer periodicity opens thus the possibility to engineer Dirac fermions in various semiconductor compounds. Tight-binding calculations are under way to reveal the electronic sub-bands of the two-dimensional PbSe sheets with a square and honeycomb structure as shown in Figure 4.

While we demonstrated geometric control with nanocrystals of the lead–chalcogenide family, we should remark that the formed one- and two-dimensional semiconductors can be further transformed to other semiconductor compounds by means of cation exchange, while the overall geometry and crystallinity is preserved. For instance, in Figure 4c we showed that the ultrathin PbSe rocksalt sheets can be converted into CdSe zinc blende sheets with preservation of the square nanostructuring. In the SI, Figure S16, we show the conversion of the CdSe sheets to Cu<sub>2–x</sub>Se sheets. The latter compound opens the gate to use cation exchange to obtain low-dimensional superlattices of various semiconductor compounds.<sup>25–28</sup> Hence, we showed that the low-dimensional PbSe structures prepared by oriented attachment can be transformed to many other compounds while the overall superlattice geometry is preserved. Although many 2-D semiconductors can also be prepared by precious gas-phase methods, the latter methods often do not allow to obtain a superlattice structure with periodicity in the nanometer region, such as the ones we present in Figure 4.

In summary, we have presented results that show that the process of oriented attachment of PbSe nanocrystals can be controlled by simple reaction parameters, resulting in single-crystalline PbSe nanostructures with dimensions between 1 and

3. The ultrathin 2-D sheets are single crystalline and show a super periodicity with planar square or honeycomb geometry. The structures can be picked up on a substrate of choice and can even be transformed to other semiconductor compounds preserving the overall geometry.

## ■ ASSOCIATED CONTENT

### 📄 Supporting Information

Additional experimental results and methods are available, including synthesis, characterization of the shapes, oriented attachment of PbSe rods and stars, study of defects and conversion of PbSe sheets to CdSe or Cu<sub>2–x</sub>Se sheets by ion exchange. Additionally, a theoretical study of the adsorption of PbSe cubes on a liquid–air interface is given. This material is available free of charge via the Internet at <http://pubs.acs.org>.

## ■ AUTHOR INFORMATION

### Corresponding Author

\*E-mail: [d.vanmaekelbergh@uu.nl](mailto:d.vanmaekelbergh@uu.nl).

### Notes

The authors declare no competing financial interest.

## ■ ACKNOWLEDGMENTS

We wish to acknowledge C. B. Murray for useful discussions. We also wish to acknowledge J. D. Meeldijk for the TEM-EDX measurements. W.H.E., M.C., and D.V. wish to acknowledge NWO-CW for financial support (Topgrant 700.53.308 and Vidi Grant No. 700.56.423). D.V. also acknowledges the Dutch FOM (FP/AV-09.0224) and the European Union under the Seventh Framework Program for financial support (ITN Herodot). S.B. and B.G. are grateful to the Fund for Scientific Research—Flanders and acknowledge financial support from the European Union under the Seventh Framework Program (Integrated Infrastructure Initiative No. 262348 European Soft Matter Infrastructure, ESMI). The authors also acknowledge financial support from the Flemish Hercules 3 programme for large infrastructure. M.D. acknowledges financial support by a NWO Vici Grant and R.v.R. by the Utrecht University High Potential Programme.

## ■ REFERENCES

- (1) Banfield, J. F.; Welch, S. A.; Zhang, H. Z.; Ebert, T. T.; Penn, R. L. *Science* **2000**, 289 (5480), 751–754.
- (2) Niederberger, M.; Colfen, H. *Phys. Chem. Chem. Phys.* **2006**, 8 (28), 3271–3287.
- (3) Zheng, H.; Smith, R. K.; Jun, Y.-w.; Kisielowski, C.; Dahmen, U.; Alivisatos, A. P. *Science* **2009**, 324 (5932), 1309.
- (4) Cho, K. S.; Talapin, D. V.; Gaschler, W.; Murray, C. B. *J. Am. Chem. Soc.* **2005**, 127 (19), 7140–7147.
- (5) Yu, Z.; Liu, B.; Ye, B.; Kong, W.; Weng, J.; Wang, Z.; Wang, H. *Rare Metal Mater. Eng.* **2010**, 39, 133–137.
- (6) Pacholski, C.; Kornowski, A.; Weller, H. *Angew. Chem., Int. Ed.* **2002**, 41 (7), 1188.
- (7) Schliehe, C.; Juarez, B. H.; Pelletier, M.; Jander, S.; Greshnykh, D.; Nagel, M.; Meyer, A.; Foerster, S.; Kornowski, A.; Klinke, C.; Weller, H. *Science* **2010**, 329 (5991), 550–553.
- (8) Xu, F.; Ma, X.; Gerlein, L. F.; Cloutier, S. G. *Nanotechnology* **2011**, 22 (26), 265604.
- (9) Koh, W. K.; Bartnik, A. C.; Wise, F. W.; Murray, C. B. *J. Am. Chem. Soc.* **2010**, 132 (11), 3909–3913.
- (10) Manna, L.; Milliron, D. J.; Meisel, A.; Scher, E. C.; Alivisatos, A. P. *Nat. Mater.* **2003**, 2 (6), 382–385.
- (11) Yin, Y.; Alivisatos, A. P. *Nature* **2005**, 437 (7059), 664–670.
- (12) Zhang, J.; Huang, F.; Lin, Z. *Nanoscale* **2010**, 2 (1), 18–34.

- (13) Evers, W. H.; De Nijs, B.; Filion, L.; Castillo, S.; Dijkstra, M.; Vanmaekelbergh, D. *Nano Lett.* **2010**, *10* (10), 4235–4241.
- (14) Dong, A. G.; Chen, J.; Vora, P. M.; Kikkawa, J. M.; Murray, C. B. *Nature* **2010**, *466* (7305), 474–477.
- (15) Bals, S.; Casavola, M.; van Huis, M. A.; Van Aert, S.; Batenburg, K. J.; Van Tendeloo, G.; Vanmaekelbergh, D. *Nano Lett.* **2011**, *11* (8), 3420–3424.
- (16) Fang, C. M.; van Huis, M. A.; Vanmaekelbergh, D.; Zandbergen, H. W. *ACS Nano* **2010**, *4* (1), 211–218.
- (17) Pieranski, P. *Phys. Rev. Lett.* **1980**, *45* (7), 569–572.
- (18) Schapotschnikow, P.; van Huis, M. A.; Zandbergen, H. W.; Vanmaekelbergh, D.; Vlugt, T. J. H. *Nano Lett.* **2010**, *10* (10), 3966–3971.
- (19) Talapin, D. V.; Black, C. T.; Kagan, C. R.; Shevchenko, E. V.; Afzali, A.; Murray, C. B. *J. Phys. Chem. C* **2007**, *111* (35), 13244–13249.
- (20) Talapin, D. V.; Murray, C. B. *Science* **2005**, *310* (5745), 86–89.
- (21) Akhmerov, A. R.; Beenakker, C. W. J. *Phys. Rev. B* **2008**, *77* (8), 085423–085433.
- (22) Park, C.-H.; Yang, L.; Son, Y.-W.; Cohen, M. L.; Louie, S. G. *Phys. Rev. Lett.* **2008**, *101* (12), 126804.
- (23) Park, C.-H.; Louie, S. G. *Nano Lett.* **2009**, *9* (5), 1793–1797.
- (24) Gomes, K. K.; Mar, W.; Ko, W.; Guinea, F.; Manoharan, H. C. *Nature* **2012**, *483* (7389), 306–310.
- (25) Li, H.; Brescia, R.; Krahne, R.; Bertoni, G.; Alcocer, M. J. P.; D'Andrea, C.; Scotognella, F.; Tassone, F.; Zanella, M.; De Giorgi, M.; Manna, L. *ACS Nano* **2012**, *6* (2), 1637–1647.
- (26) Jain, P. K.; Amirav, L.; Aloni, S.; Alivisatos, A. P. *J. Am. Chem. Soc.* **2010**, *132* (29), 9997–9999.
- (27) Li, H.; Zanella, M.; Genovese, A.; Povia, M.; Falqui, A.; Giannini, C.; Manna, L. *Nano Lett.* **2011**, *11* (11), 4964–4970.
- (28) Jain, P. K.; Beberwyck, B. J.; Fong, L.-K.; Polking, M. J.; Alivisatos, A. P. *Angew. Chem., Int. Ed.* **2012**, *51* (10), 2387–2390.

# Supporting Information

## **Low-dimensional semiconductor superlattices formed by geometric control over nanocrystal attachment: Experimental results**

W. H. Evers, B. Goris, S. Bals, M. Casavola, J. de Graaf, R. van Roij, M. Dijkstra and D.

Vanmaekelbergh

- I Experimental section on synthesis and oriented attachment**
- II Characterization of the shape and the facets of the PbSe nanocrystals by HAADF-STEM**
- III Effect of the crystal size on the attachment of PbSe nanocubes.**
- IV Overview of the structures formed by oriented attachment in a hexane dispersion**
- V Effect of addition of oleic acid capping molecules to the ethylene glycol**
- VI HAADF-STEM study of defects in oriented attachment**
- VII Oriented attachment of PbSe rods and stars**
- VIII Conversion of PbSe sheets to CdSe or  $\text{Cu}_{2-x}\text{Se}$  sheets by ion exchange**
- IX XRD analysis of the structures formed by oriented attachment**
- X GISAXS study of the oriented attachment in the glycol-ethylene/suspension reactor system**

## I Experimental section on synthesis and oriented attachment

*PbSe nanocubes*: PbSe nanocubes were synthesized by a method described by Houtepen *et al*<sup>[1]</sup>. The synthesis was performed in a water and oxygen free environment. (1) 1.9 gram of lead acetate tri hydrate (99.999% Aldrich), 4 mL of diphenyl ether (99% DPE, aldrich), 3 mL of oleic acid (OA, 90% Aldrich) and 16 mL trioctyl phosphine (TOP, 90% Fluka) were heated to 100 °C under low pressure ( $10^{-3}$  bar) for ~3 hours. (2) A second mixture containing 0.31 g Se (99.999% Alfa Aesar) and 4 mL TOP was prepared. Subsequently 11.5 mL of solution (1) and 1.7 ml of solution (2) was injected into 10 mL 190 °C DPE. The reaction mixture was kept at a constant temperature of 145 °C. After 30 seconds to 10 minutes the reaction mixture was quenched with 20 mL butanol and 10 mL methanol. The crude synthesis mixtures were washed twice by precipitating with methanol, centrifugation and redispersion of the sediment in toluene. This resulted in PbSe nanocrystals with a truncated cubic shape, as shown below.

*PbSe stars*: In order to obtain PbSe “stars”, the synthesis procedure was adapted as follows: During the first step in the PbSe nanocrystal synthesis, i.e. the preparation of Pb-oleate precursor, the precursor was only allowed to react for ~30 minutes. Hence a small amount of acetic acid remained in the precursor mixture. The acetic acid facilitates the growth of PbSe nanostars.<sup>[1]</sup>

*PbSe rods*: rods were prepared as follows: the Pb-oleate and TOP-Se precursors were prepared as described above. 9 ml of the Pb-oleate precursor solution was injected into 13 ml DPE at 190 °C. After one minute, 0.6 ml of the TOP-Se solution was injected and the reaction was allowed to proceed for 20 minutes at a constant temperature of 140 °C. Both quenching of the reaction and purification of the NCs were performed as described above.<sup>[2]</sup>

Oriented attachment was achieved by slow evaporation of the solvent from the nanocrystal suspension placed on top of ethylene glycol as an immiscible liquid substrate, at a given temperature (called the reaction temperature). In a typical experiment, 1 mL of ethylene glycol was placed in a glass vial (Ø 10 mm). After the desired temperature (between 20 and 140 °C) was reached, 50 µL of nanocrystal suspension was injected after which the solvent was allowed to evaporate, as depicted in figure S1. The evaporation takes from 90 to 10 minutes. After evaporation a sample was taken from the ethylene glycol layer at the center of the vial and placed under vacuum to evaporate the residual ethylene glycol. All experiments were performed in a nitrogen purged glovebox.

The nanocrystals were imaged using high angle annular dark field scanning transmission electron microscopy (HAADF-STEM) performed using a double aberration corrected FEI TITAN operated at 300kV. The semi convergence angle of the electron probe used during acquisition was 21.4 mrad. The conventional TEM images were obtained with a FEI Tecnai 12.

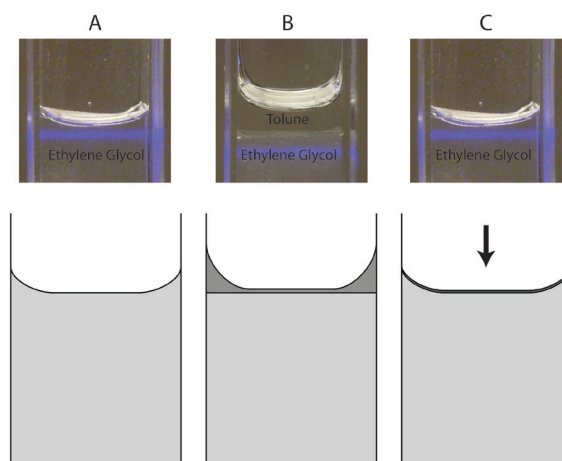


Figure S1: Cartoon of the evaporation process. Ethylene glycol is placed in a vial (A) after which the PbSe nanocrystal suspension is deposited on top of it (B). To illustrate the effect the amount of suspension has been increased tenfold in figure B. After the solvent is evaporated, a sample is taken in the centre of the vial at the air/liquid interface. The entire experiment takes place in a nitrogen purged glovebox (oxygen and water below 10 ppm).

- (1) Houtepen, A. J.; Koole, R.; Vanmaekelbergh, D.; Meeldijk, J.; Hickey, S. G. *Journal of the American Chemical Society* 2006, 128, (21), 6792-6793.
- (2). Casavola, M.; van Huis, M. A.; Bals, S.; Lambert, K.; Hens, Z.; Vanmaekelbergh, D. *Chem. Mater.* **2012**, 24 (2), 294–302.

## II Characterization of the shape and the facets of the PbSe nanocrystals by HAADF-STEM

*Nanocubes* The shape and facets of the PbSe nanocubes were investigated in detail with High Angle Annular Dark Field Scanning Transmission Electron Microscopy (HAADF-STEM). In figure S2, two HAADF-STEM images are presented, obtained from PbSe nanocrystals with a diameter of 9.9 nm. Figures S2a and S2b present images acquired with the electron beam oriented along the [110] axis and the [100] axis respectively. The edges of the projection can be identified as {100}, {011} and {111} facets. Figures (c) and (d) present intensity profiles taken along the direction indicated by the arrows in (a), showing a {100} → {110} → {100} sequence of facets in (c) and a {111} → {110} → {111} sequence in (d). These results are in line with a truncated nanocube model (see inset) with 6 natural {100} facets and {110} and {111} truncations.

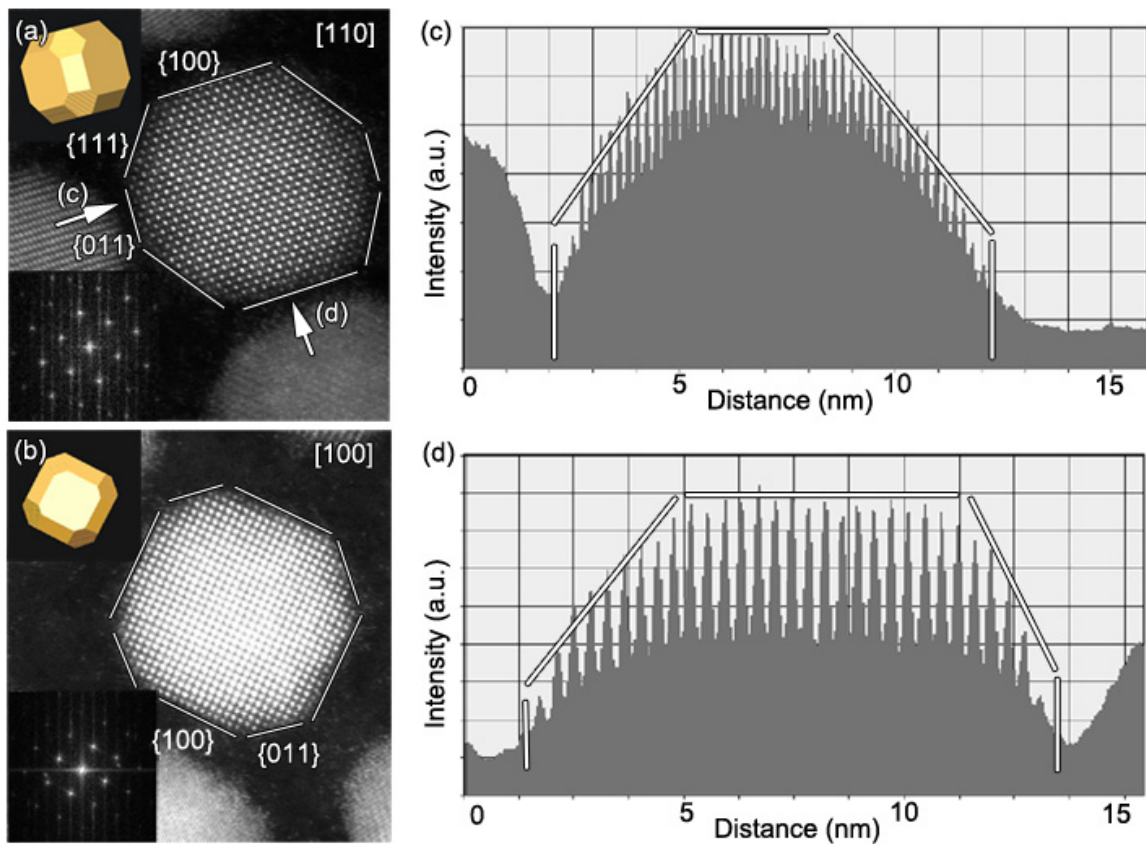
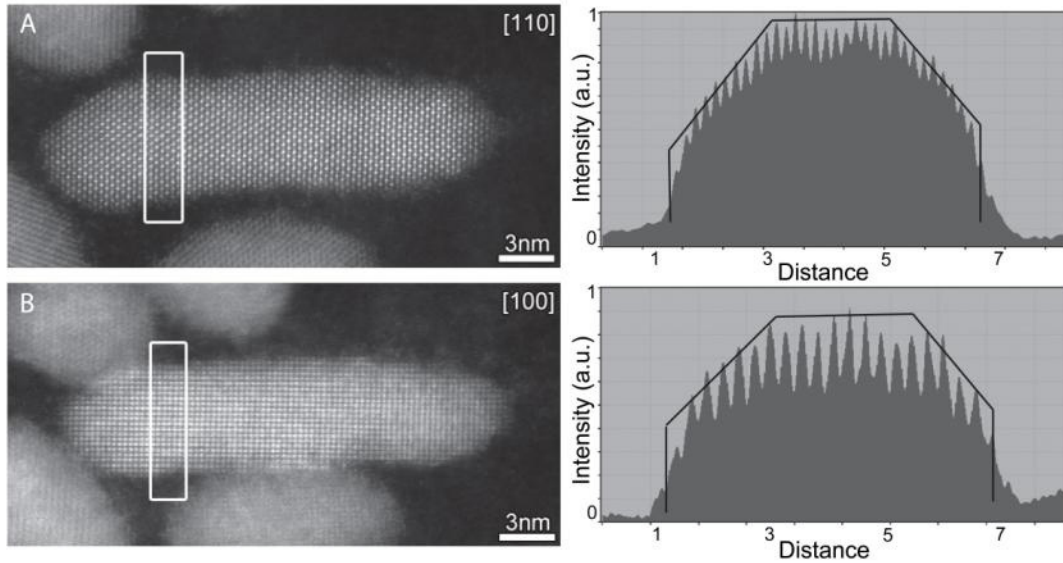


Figure S2: High resolution HAADF-STEM image of PbSe nanoparticle oriented along the [110] zone axis (a) and along the [100] zone axis (b). Both the outer shapes of the 2-D projection images and the intensity profiles (c,d) corresponds to our model of a cube with truncated {110} and {111} facets.

*Nanorods* A similar study was performed for PbSe nanorods as shown in figure S3. It was found that the tips of the nanorods yield a smooth  $\{100\}$  termination whereas the long facets are roughened  $\{100\}$  and  $\{110\}$  facets.



*Figure S3: High resolution HAADF-STEM image of PbSe nanorod oriented along the [110] zone axis (a) and along the [100] zone axis (b). Both the outer shapes of the projection and the intensity profiles corresponds to our model of a nanorod with truncated  $\{100\}$  and  $\{110\}$  facets along the long facets and  $\{100\}$  termination along the short facets.*

### III Effect of the crystal size on the attachment of PbSe nanocubes.

Various sizes of PbSe truncated nanocubes have been used in order to study the size dependence of the oriented attachment. In figures S4-S6 the structures obtained with three different sizes of PbSe NCs, with a diameter of 4.4, 7.5 and 9.9 nm, are presented. In all cases, oriented attachment leads to linear 1-D or 2-D cubic structures. However, the smallest NCs are much more reactive and show oriented attachment already at room temperature, while the 9.9 nm particles show oriented attachment at and above 100 °C only.

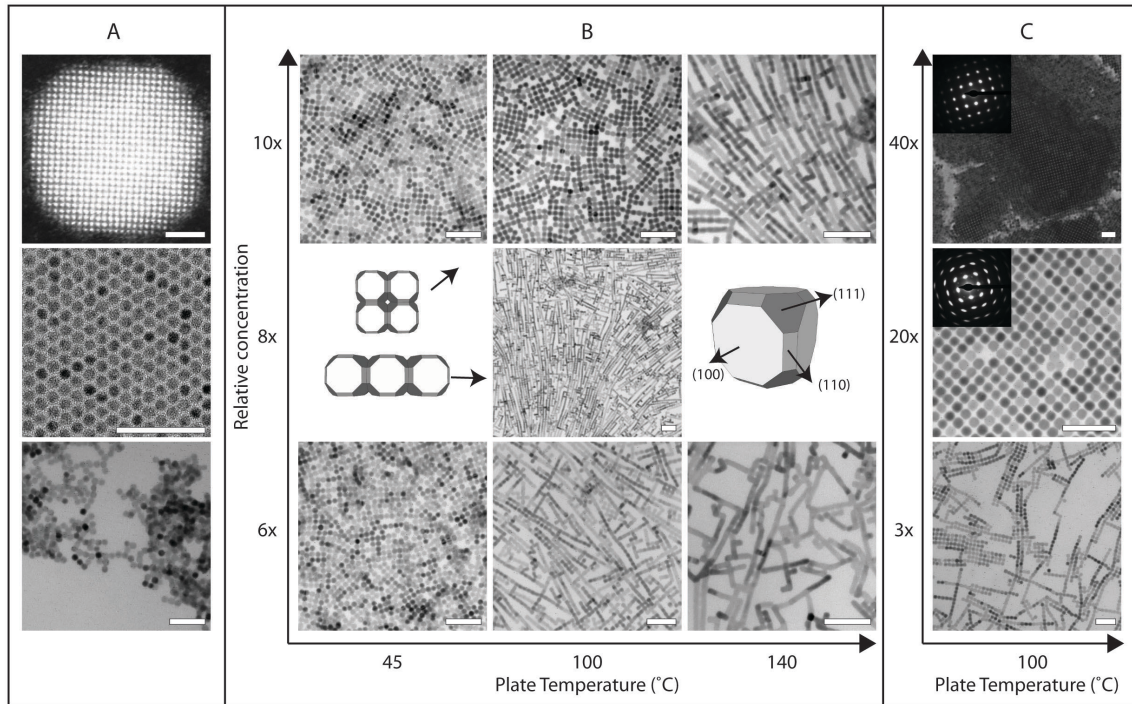


Figure S4: Overview of the obtained structures. Panel A from top to bottom; Top; 9.9 nm NC showing the truncation along the  $\{110\}$  planes. Middle; Hexagonal ordering of 7.0 nm PbSe|CdSe core shell structures on ethylene glycol at 100 °C. The CdSe acts as protection, hence no oriented attachment is observed. Bottom; Aggregates of 7.5 nm NC observed when low concentrations were used ( $<2x C_{Ref} = 140$  nM for the 7.5 nm particles). Panel B: PbSe NCs with a diameter of 7.5 nm, Panel C: PbSe NCs with a diameter of 9.9 nm. From bottom to top increasing particle concentration with respect to the lowest concentration used. The complete data set can be found in figure S5 and S6. From left to right, for panel B, increasing temperature of the reaction. At low concentrations predominately linear aggregation with two bonding sites is observed. With increasing concentration cubic ordering occurs with oriented attachment that involves 4 bonding sites. By increasing the temperature of the reaction the reversed trend can be observed, at low temperature cubic arrangement occurs while at high temperature linear attachment is predominant. From the electron diffractogram in the inset in the 2-D and 3-D structures in panel C it can be concluded that the particles are not only oriented on the NC scale but also on the atomic scale. The scale bar in the top image of panel A represents 2 nm, all other scale bars represent 50 nm.

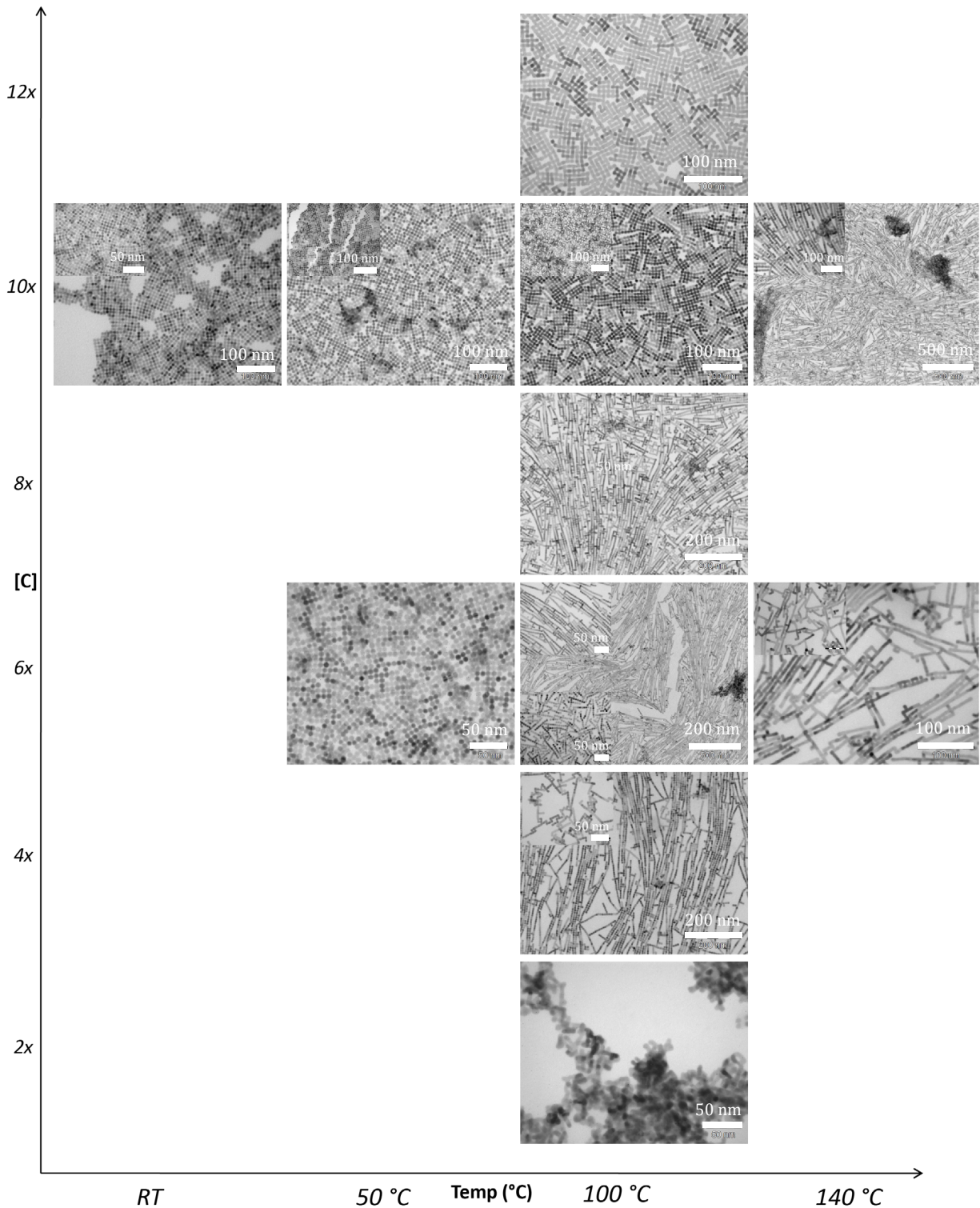


Figure S5: Oriented attachment of 7.5 nm PbSe in toluene casted on ethylene glycol at various temperatures using also different NC concentrations relative to the lowest concentration.

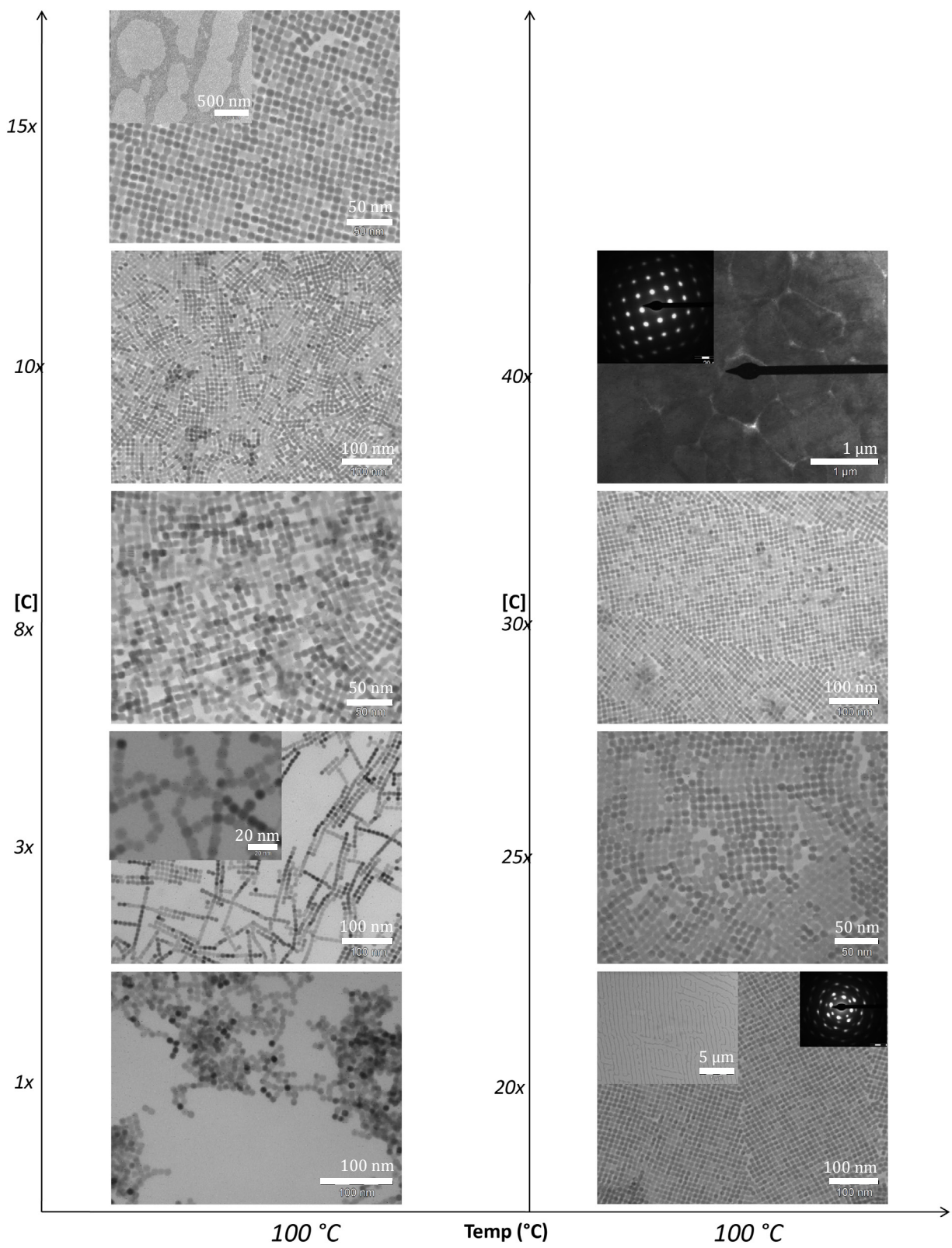


Figure S6: Oriented attachment of 9.9 nm PbSe NCs in toluene on ethylene glycol at 100 °C, using different NC concentrations relative to the lowest concentration.

#### IV Overview of the structures formed by oriented attachment in a hexane dispersion

Figure S7 presents results of experiments using PbSe NC dispersions with hexane as a solvent instead of toluene. Oriented attachment leads to the formation of 1-D wires and 2-D sheets in a similar way as with toluene as a solvent. However, with hexane as solvent, there is a tendency to form more extended cubic sheets. In addition, oriented attachment sets on at a lower temperature.

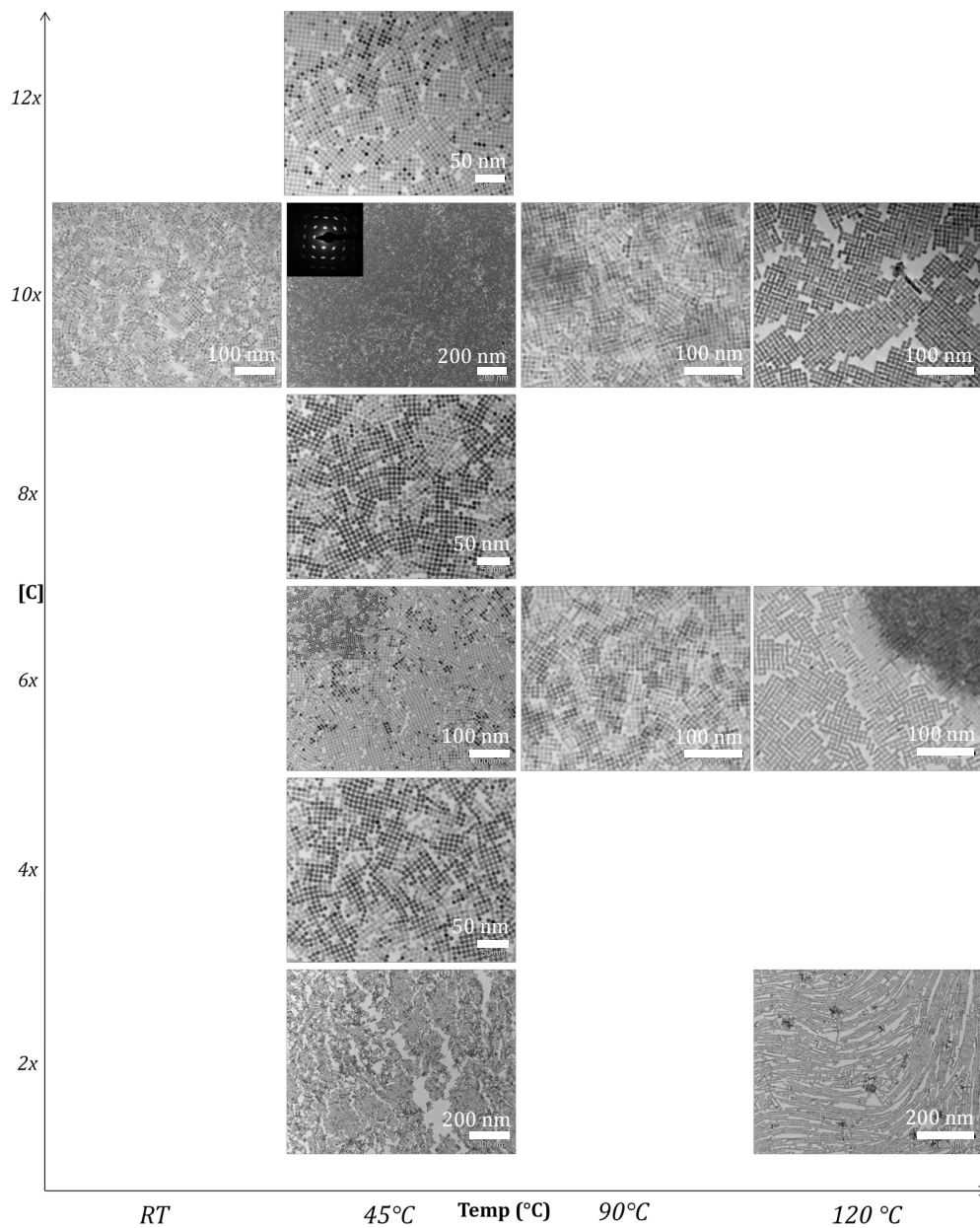


Figure S7: Oriented attachment of 7.5 nm PbSe NCs on ethylene glycol using hexane as solvent, at various temperatures and with different concentrations relative to the lowest concentration.

## V Effect of addition of oleic acid capping molecules to the ethylene glycol

The effect of oleic acid capping ligands added to the glycol phase, for different concentrations of the nanocrystals, is presented in figure S8. We used 5.4 nm PbSe nanocrystals. 50  $\mu\text{L}$  of the nanocrystal suspension was injected in a 78.5  $\text{mm}^2$  reaction vessel containing 1 mL ethylene glycol. If no capping was added, it can be observed that for this size nanocrystals a honeycomb type-structure exist at a concentration of  $\sim 11\text{-}20$  mol/L. The honeycomb structure is always in equilibrium with the rod-like structures. When additional capping ligands were added oriented attachment is not observed, typical hexagonal self-assembly is achieved instead. When even more ligands were added large crystallites were observed as is shown in the insets. The same trend was observed when n-tetradecyl phosphonic acid or octadecyl phosphonic acid was used as additional capping ligands (see figure S9)

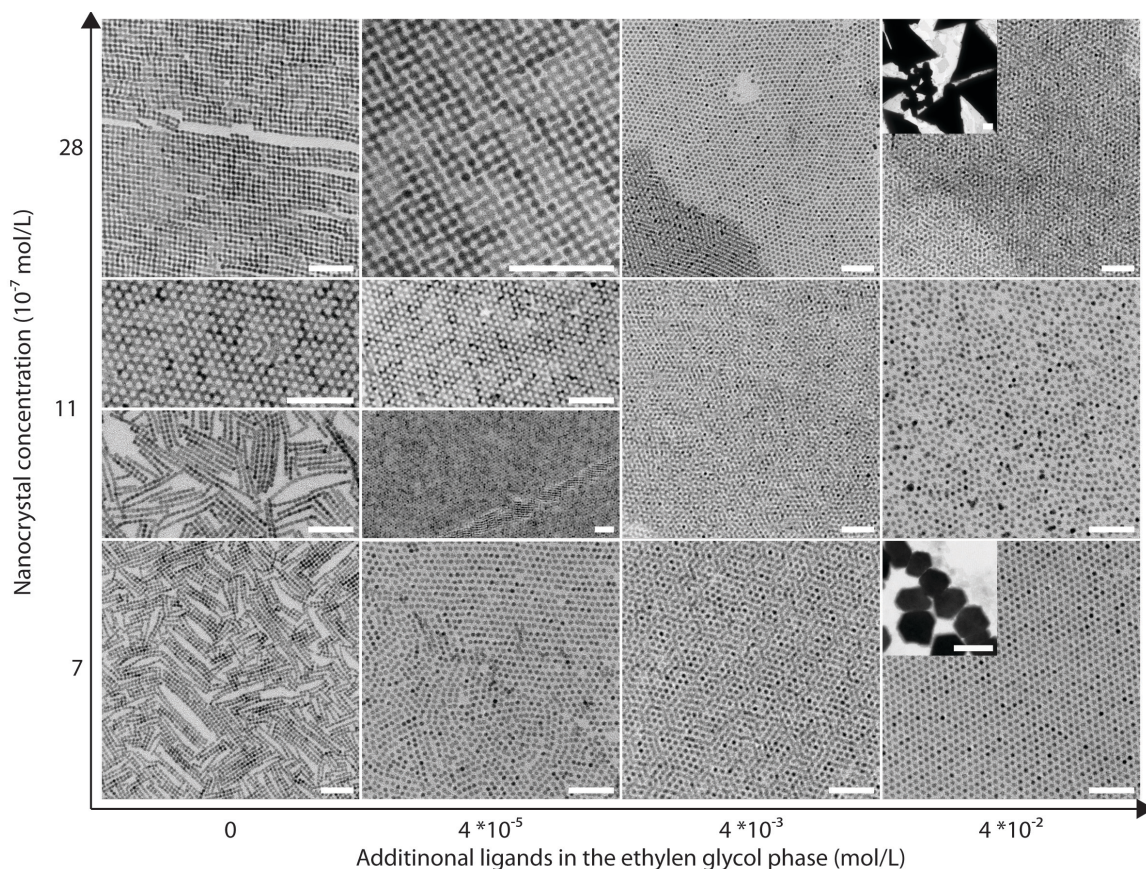
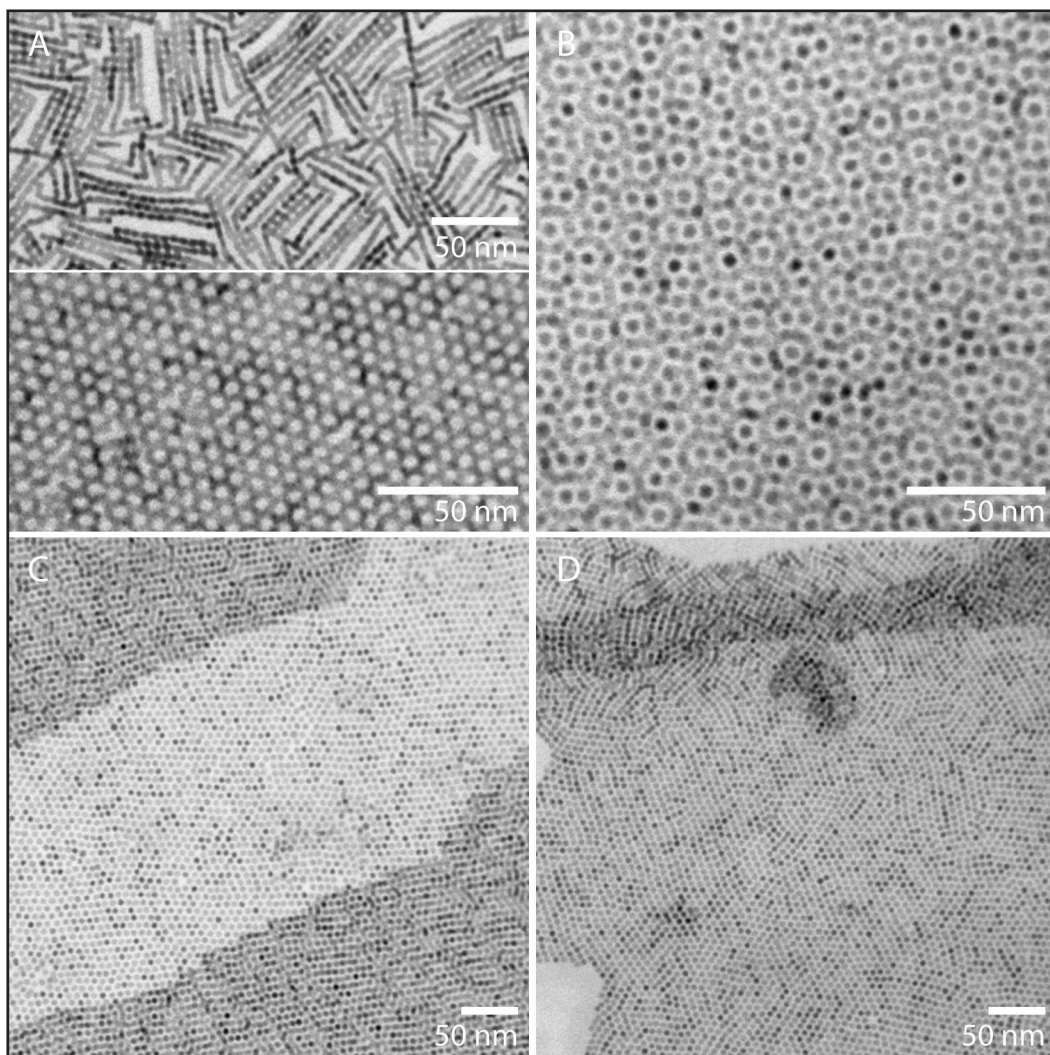


Figure S8: Effect of additional oleic acid capping ligands in the glycol phase as function of the nanocrystal concentration for 5.4 nm PbSe nanocrystals. The scale bars represent 50 nm except for the insets where they represent 1  $\mu\text{m}$ .



*Figure S9: Effect of various capping ligands to the ethylene glycol phase. A) no additional ligands. B) Addition of  $4 \cdot 10^{-4}$  mol/L oleic acid. C) Addition of  $4 \cdot 10^{-4}$  mol/L n-tetradecyl phosphoric acid. D) Addition of  $4 \cdot 10^{-4}$  mol/L octadecyl phosphoric acid.*

## VI HAADF-STEM study of defects in oriented attachment

The irreversible strong bonding of the nanocrystals by oriented attachment leads inherently to imperfect attachment events. Imperfect attachment induces crystal defects during the growth<sup>[3]</sup>. In the case reported here, oriented attachment does not always occur by connection of two perfectly aligned {100} facets. Figure S10A shows two attached nanocubes, their opposed {100} planes were, however, not completely parallel resulting in an edge dislocation. Figure S10B shows another defective way of attachment: the nanocubes in the linear structure have parallel {100} bonding facets; they are, however, all differently rotated in the plane perpendicular to the bond axis.

When the structures formed by oriented attachment were thermally treated under nitrogen, remarkable atomic reconfigurations were observed in which the effects of misorientations were annealed, and the original shape of the building blocks is gradually washed out. A part of a nearly perfectly smooth PbSe sheet obtained by oriented attachment and thermal annealing is presented in Figure S10C; only a small trace of the early connection of two nanocrystals is still visible. The results of oriented attachment of small PbSe nanocubes at 50 °C, and further annealing are presented in Fig. S11. Panel A shows a planar sheet formed by oriented attachment of PbSe nanocubes 5.4 nm in diameter; the structure that constitutes an atomic PbSe rocksalt single crystal still shows the signature of the original building blocks. If oriented attachment is followed by a thermal treatment at 80 °C, a further atomic smoothing is observed leading to a two-dimensional network in which the original nanocubes can no longer be recognized.

(3) Penn, R. L.; Banfield, J. F. *Science* **1998**, 281, (5379), 969-971.

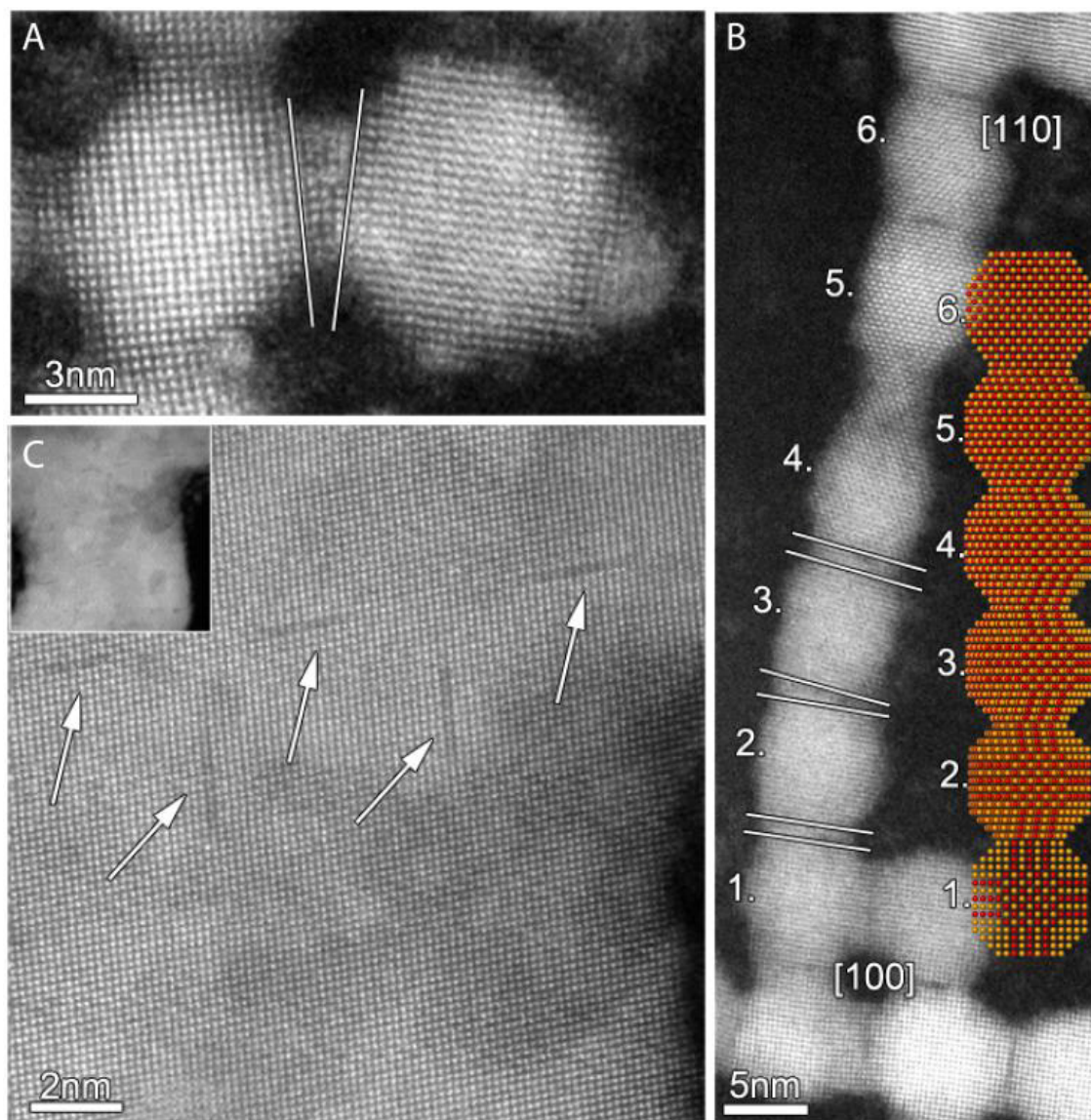
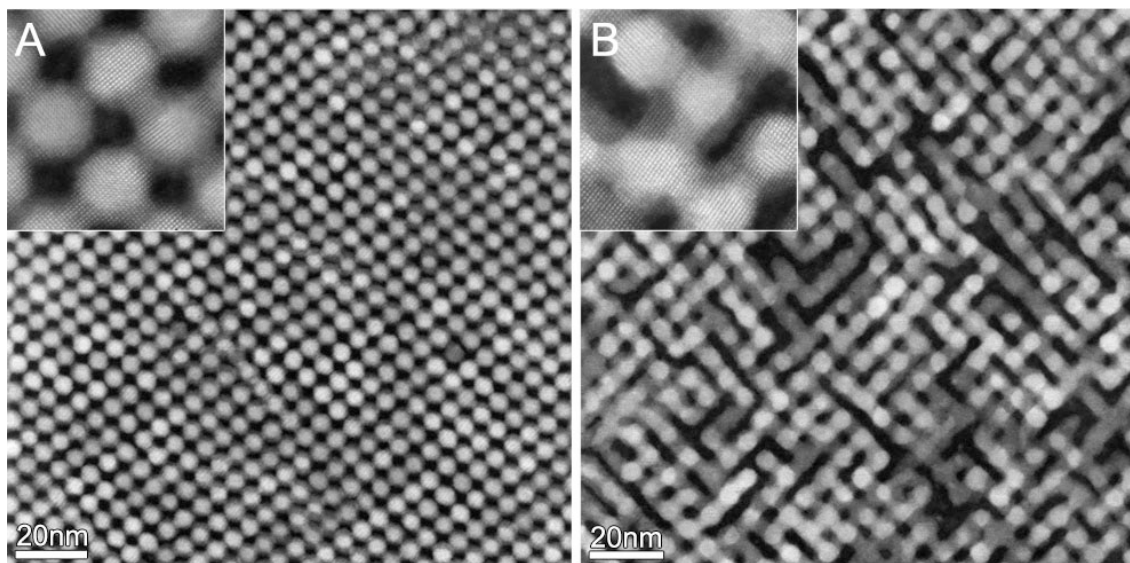


Figure S10: Imperfect oriented attachment of PbSe nanocrystals. A) Two attached NC with their  $\{100\}$  planes being not completely parallel, resulting in an edge dislocation. B) The NCs are rotated over  $45^\circ$  over 6 particles in respect to the bonding axis, resulting in a screw dislocation. C) Nearly defect free single-crystalline sheet with a nearly homogenous thickness and lateral dimensions in the  $\mu\text{m}$  range. The arrow indicates missing rows where the original particles were situated. The particles used in A and B were 7.5 nm PbSe NCs while in C 9.9 nm PbSe NCs were used.



*Figure S11: The fusing process of 5.4nm PbSe nanocrystals. Both samples were similarly grown at 50 °C for which a single crystalline square lattice was obtained as given in figure A. After evaporation the temperature was increased to 80 °C for figure B.*

## VII Oriented attachment of PbSe rods and stars

*PbSe rods* Besides the oriented attachment of truncated cubic PbSe NCs, we also studied the oriented attachment of PbSe nanorods and nanostars. The rods have smooth  $\{100\}$  facets on both the tips; the long-side facets also correspond to  $\{100\}$ , but there is considerable roughening. Figure S12 shows a sample before and after attachment took place. It is evident that the rods only attach with the  $\{100\}$  tip facets forming strings of rods, and that the rough side-facets are not used in the attachment. This is possibly caused by the roughening of these facets that also could lead to a stronger absorption of the surfactant molecules. The formation of exclusively 1-D structures was observed in broad range of temperature and concentration.

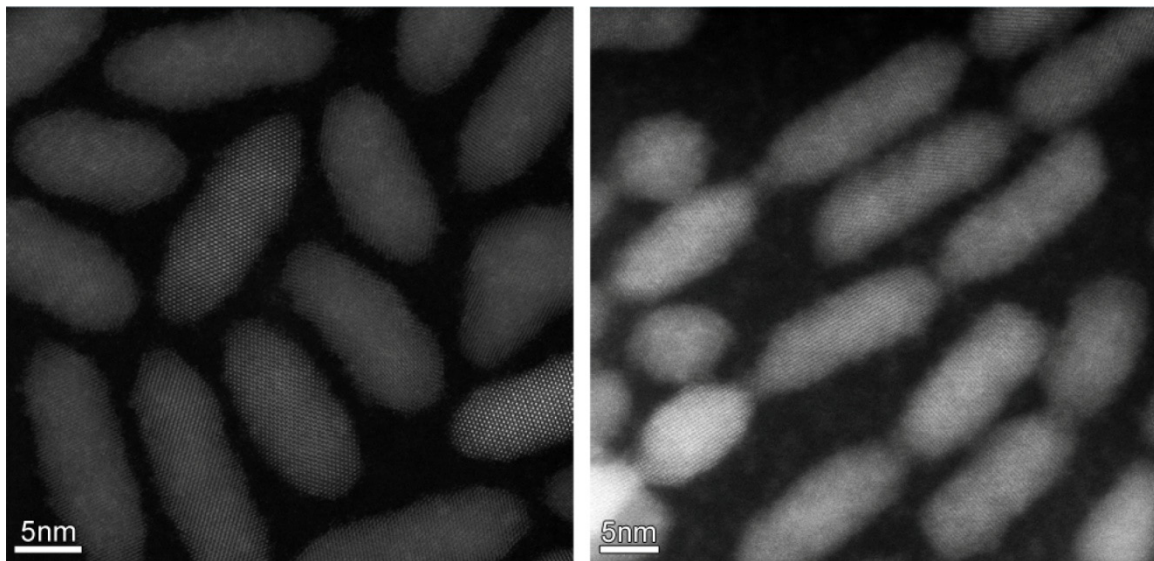


Figure S12: Linear oriented attachment of PbSe nanorods. Left: drop casted nanorods, and right a picture after solvent evaporation at a temperature of 20 °C, leading to attachment via the  $\{100\}$  tips.

*PbSe stars* Nanostars were synthesised as in Ref. 1, and used in experiments of oriented attachment. These stars have 8 tips that presumably end as very small  $\{100\}$  facets. Oriented attachment of PbSe nanostars resulted in cubic- and wire-like arrangement of the stars, depending on the growth temperature. As can be seen in figure S13, individual PbSe stars are usually ‘lying’ on a side. A temperature increase led to oriented attachment, resulting in a cubic architecture, which was, however, less ordered than in the case of nanocubes. In these square architectures, the stars stand upright and were exclusively connected via their tips, presumably being small  $\{100\}$  end-facets. When a higher temperature was used for solvent evaporation, more wire-like structures are observed, in a similar way for the truncated cubes (see figure S13 and S14).

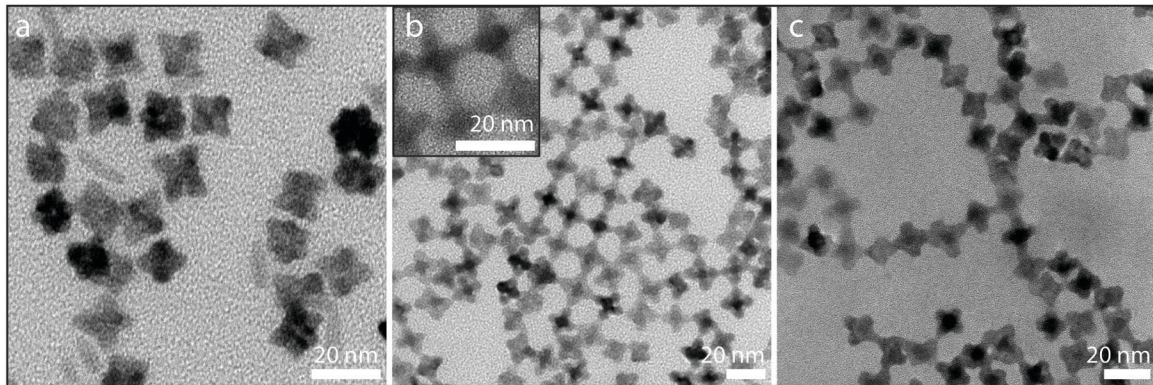


Figure S13: TEM study on the oriented attachment of PbSe nanostars. a, drop casted sample. b, oriented attachment grown at 100 °C. c, oriented attachment grown at 150 °C.

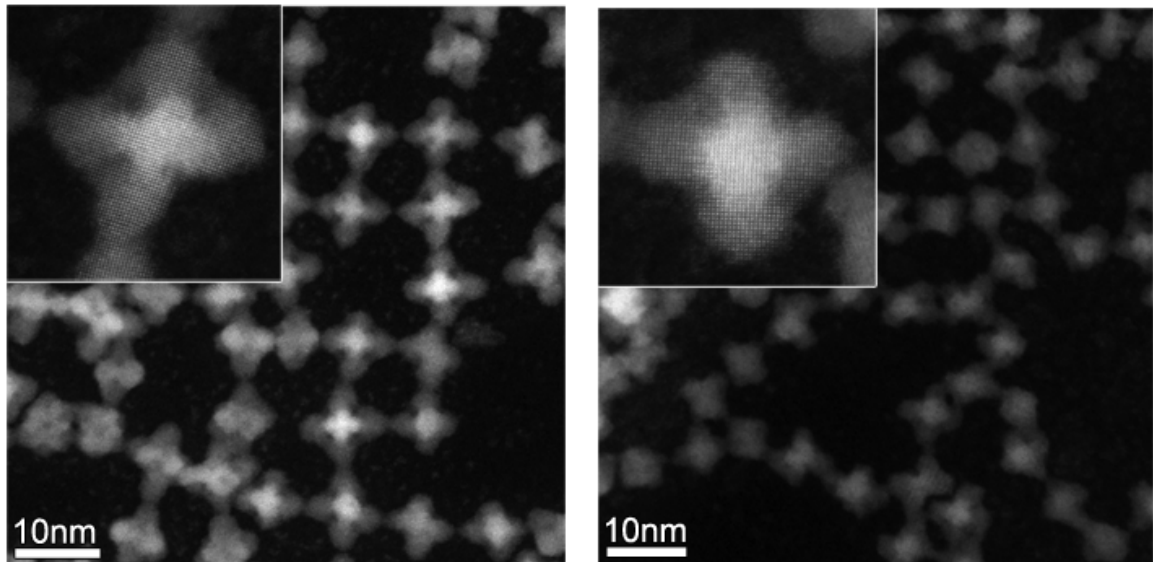


Figure S14: In-depth HAADF-STEM study on the oriented attachment of PbSe nanostars. Left a sample grown at 100 °C and right a sample grown at 150 °C.

## VIII Conversion of PbSe sheets to CdSe or Cu<sub>2-x</sub>Se sheets by ion exchange

The conversion of a PbSe sheet into a CdSe sheet was obtained by placing the PbSe sheet on a substrate (TEM-grid or silicon (100) wafer), which was then brought in contact with a 0.1 M Cd-oleate solution in 1-octadecene and heated up to 130 °C for 2 hours. The results presented in figure S15 provide evidence that the sheets preserve their cubic particle symmetry, while from the electron diffraction patterns and SEM-EDX results it follows that the atomic lattice was changed completely from rocksalt to zinc blende. SEM-EDX spectra show that the sheets are transformed from a PbSe to a CdSe composition. The electron diffraction pattern of the CdSe sheets corresponds with zinc blende CdSe with unit cell vectors ( $a=b=c$ ) of 5.873 nm<sup>[4]</sup> instead of the typical 6.050 nm<sup>[5]</sup>. Note that zinc blende CdSe with these parameters were also reported in the literature<sup>[6]</sup>. In the tables given with the radial intensity plots of the diffraction patterns (middle of figure S15), the measured values are compared with the values from literature. A good agreement can be observed for both the PbSe and the CdSe values. Strikingly, one diffraction peak of the CdSe sheets could not be fitted, and its origin remains unclear thus far.

The conversion of PbSe sheets into Cu<sub>2-x</sub>Se was obtained by first converting the PbSe sheet to a CdSe sheet as described above.<sup>[7]</sup> After the CdSe exchange the TEM grids were placed in a 2 mL 0.03M solution of tetrakis(acetonitrile)copper(I) hexafluorophosphate in methanol for 1 min, after which they were rinsed with toluene and methanol. The results in figure S16 provide evidence that the sheets preserved their cubic particle symmetry, while from the TEM-EDX results it follows that the atomic lattice is changed to Cu<sub>2-x</sub>Se.

(4). JCPDS-ICCD, **2010**, card no. 04-012-6324

(5). JCPDS-ICCD, **2010**, card no. 01-073-6987

(6). JCPDS-ICCD, **2010**, card no. 00-006-0354

(7). P. K. Jain, L. Amirav, S. Aloni, A. P. Alivisatos, *Journal of the American Chemical Society* **2010**, 132, 9997.

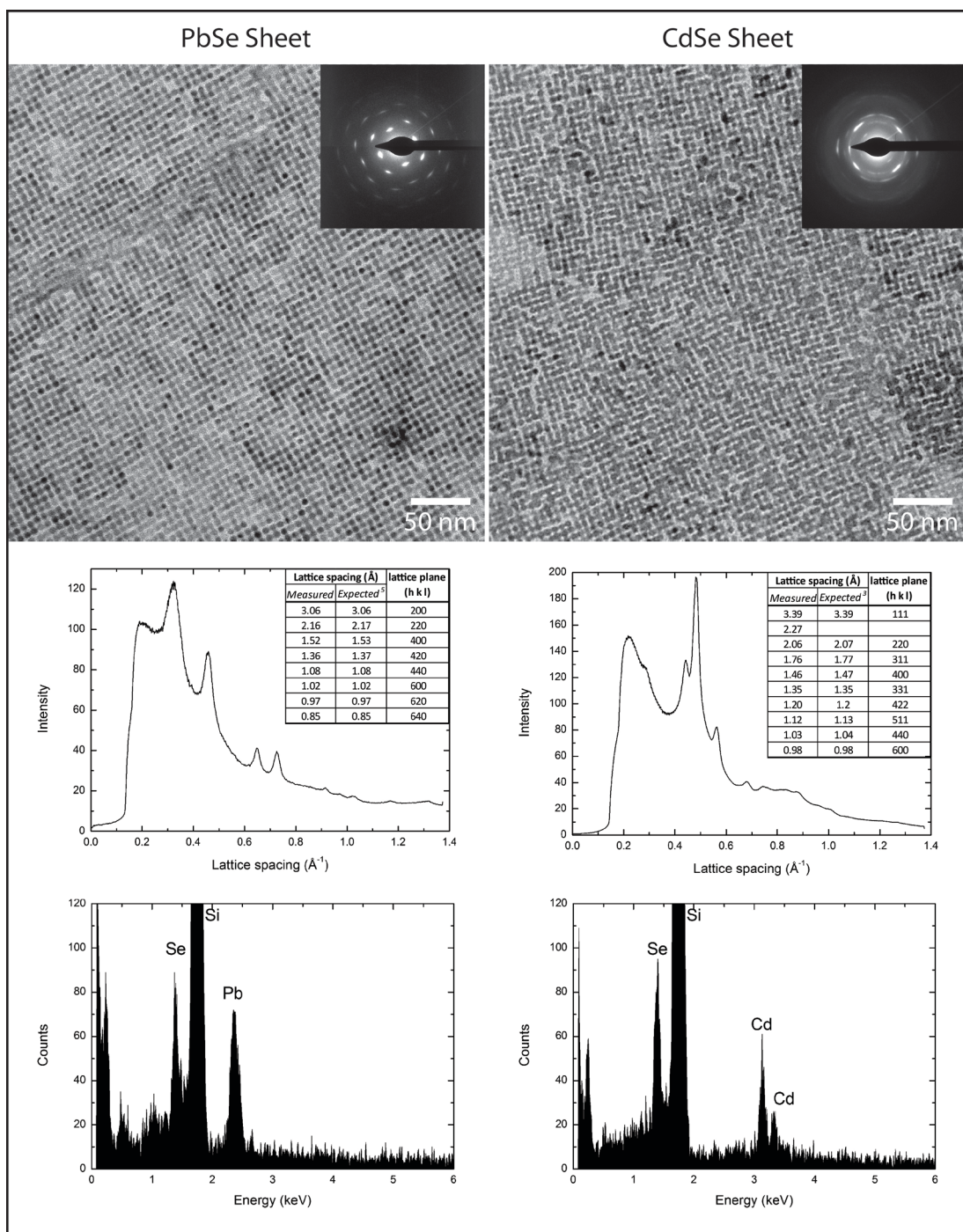


Figure S15: TEM-images, electron diffractograms and EDX measurements of a PbSe sheet, and a CdSe sheet resulting from a Cd-for-Pb cation exchange reaction starting from a PbSe sheet. From top to bottom: TEM-images, radial intensity plots of the electron diffraction patterns given in the insets, and the corresponding values for the measurement and literature, and SEM-EDX measurements of a comparable sample in a SEM.

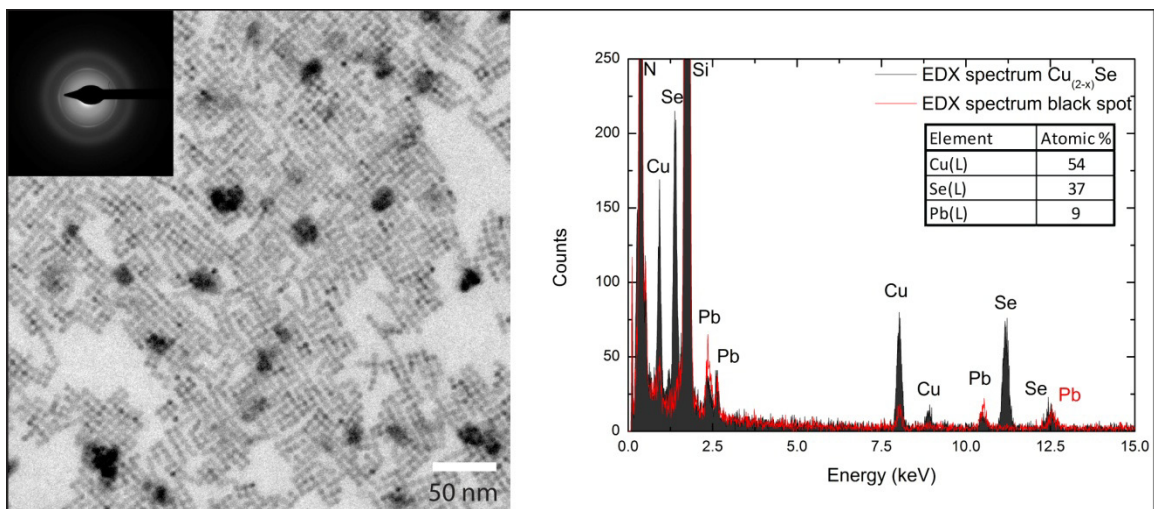


Figure S16: TEM image and TEM-EDX spectrum of the obtained structure after cation exchange with  $\text{Cu}^+$ . The EDX spectrum of the NC (black) shows both Cu, Se and some residual Pb ions while the black spots in the TEM image are composed out of Pb and Cu.

## IX XRD analysis of the structures formed by oriented attachment

In figure S17 we present XRD results of the 2-D structures formed by oriented attachment compared to those of individual unreacted nanocrystals. The wavelength used for the XRD measurements was  $1.54 \text{ \AA}$  and the spot size was approximately  $25 \text{ mm}^2$ . For the drop-casted unreacted sample, the diffraction peaks of several planar facets can be observed i.e. the NCs are randomly oriented on the substrate. The sample after oriented attachment shows mainly the (200) and to a smaller extent the (220) peaks. This indicates that in the reacted structure nearly all  $\{100\}$  facets are perpendicular to the surface, in agreement with 2-D attachment via the four upstanding  $\{100\}$  facets.

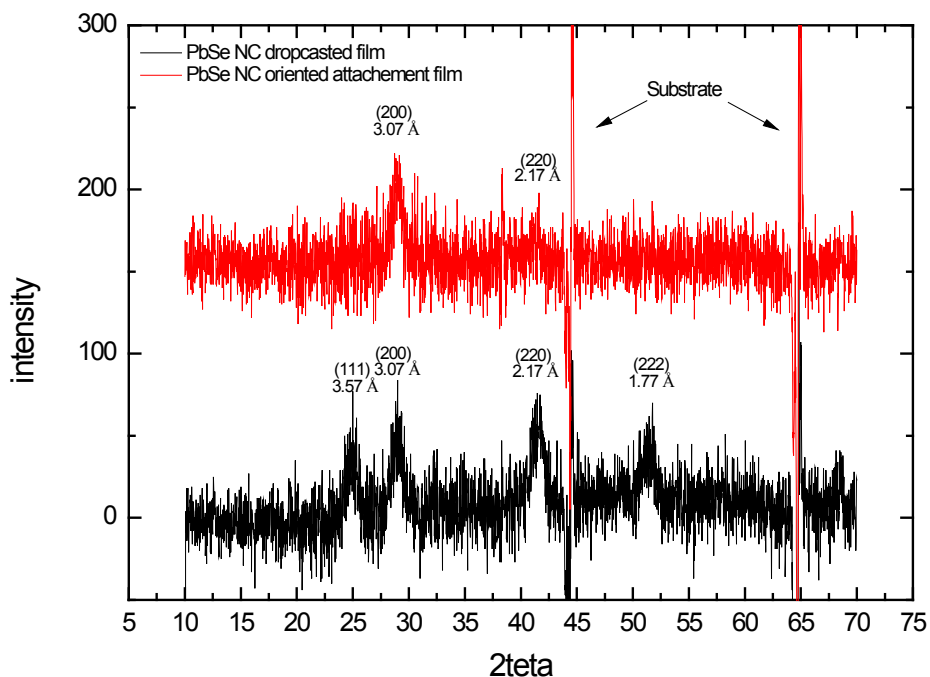


Figure S17: XRD pattern of truncated nanocubes that are drop-casted (black), and after solvent evaporation at elevated temperature leading to oriented attachment (red). The drop casted sample clearly shows several diffraction peaks due to different orientations of the NCs on the substrate, while the oriented film mainly shows the diffraction peaks of the (200) planes, showing preferential orientation of the cubes in the 2-D sheets.

## X GISAXS study of the oriented attachment in the glycol-ethylene/suspension reactor system

In-situ GISAXS measurements have been performed to study the assembly process in more detail. The measurements were carried out in the synchrotron center in Grenoble at beamline ID10 under experiment SC-3300. During and after the evaporation of the toluene, GISAXS measurements were performed with the x-ray spot probing the liquid-air interface. In figure S16 an example of a GISAXS pattern after evaporation of the solvent is presented. Diffraction peaks at a  $Q$  value of  $0.624 \text{ nm}^{-1}$  indicate ordered domains of the PbSe 9.9 nm cubes on the glycol; the average inter-particle distance is measured to be 10.1 nm, indicating that ligand-free facets are attached.

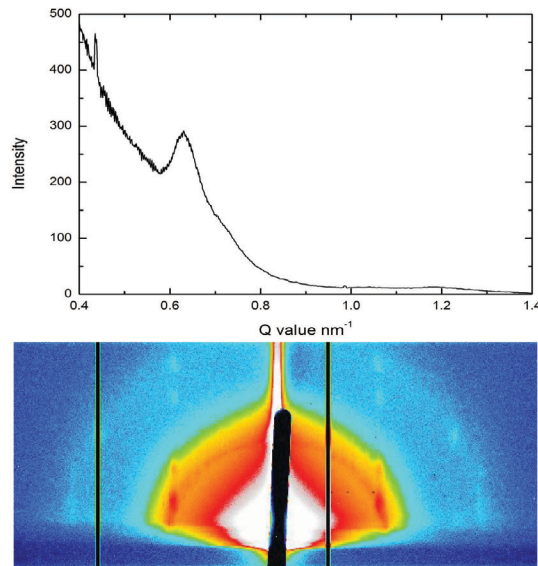


Figure S18: In-situ GISAXS pattern and corresponding intensity vs. wave-vector graph of a structure formed of 9.9 nm PbSe NCs after complete evaporation of the solvent. From the graph a dominant peak at a  $Q$ -value of  $0.64 \text{ nm}^{-1}$  can be observed.

**Low-Dimensional Semiconductor Superlattices Formed by  
Geometric Control over Nanocrystal Attachment:  
Supporting Information for the Theoretical Study**

W. H. Evers,<sup>1</sup> B. Goris,<sup>2</sup> S. Bals,<sup>2</sup> M. Casavola,<sup>1</sup> J. de Graaf,<sup>1</sup> R. van Roij,<sup>3</sup> M. Dijkstra,<sup>1</sup> and D. Vanmaekelbergh<sup>1,\*</sup>

<sup>1</sup>*Soft Condensed Matter, Debye Institute for Nanomaterials Science,  
Utrecht University, Princetonplein 1, 3584 CC Utrecht, The Netherlands*

<sup>2</sup>*EMAT, Dept. of Physics, University of Antwerpen,  
Groenenborgerlaan 171, 2010 Antwerpen, Belgium*

<sup>3</sup>*Institute for Theoretical Physics, Utrecht University,  
Leuvenlaan 4, 3584 CE Utrecht, The Netherlands*

(Dated: July 27, 2012)

## INTERFACIAL ADSORPTION OF A TRUNCATED CUBE

In this section we consider the adsorption of a single truncated (nano)cube at a flat toluene-air interface using a theoretical model based on surface-tension arguments. We apply a model similar to that of P. Pieranski, who analysed the strength of adsorption of spherical colloids at liquid-gas and liquid-liquid interfaces [1].

### The Model for the Truncated Cubes

To describe the experimental system, we consider a truncated cube which, in its initial configuration, is given by the set of vertices

$$\{\mathbf{v}(q)\} = \frac{\mathcal{P}_D \left( (\pm 1, \pm(1-q), \pm(1-q))^T \right)}{\sqrt{4(\sqrt{3}q^2 + 6\sqrt{2}q(1-q) + 6(1-q)^2)}}, \quad (1)$$

where  $q \in [0, 1]$  is the truncation parameter, ‘ $T$ ’ indicates transposition,  $\mathcal{P}_D$  is a permutation operation that generates all permutations of each element in the set of 8 vertices spanned by the  $\pm$ -operations (which are allowed to act independently of each other). By letting  $\mathcal{P}_D$  act we obtain 48 vertices. Subsequent deletion of all duplicates reduces this set to the desired total of 24 vertices for a truncated cube with 6  $\{100\}$ , 12  $\{110\}$ , and 8  $\{111\}$  facets. The expression in the denominator ensures that the truncated cube is normalized to unit surface area. By changing the value of  $q$  the truncated cube deforms smoothly from a cube ( $q = 0$ ) to an octahedron ( $q = 1$ ) *via* a cuboctahedron ( $q = \sqrt{2}/(\sqrt{2} + 1) \approx 0.586$ ), also see Fig. 1a, which shows our model for various levels of truncation. We restrict ourselves to  $q \in [0, 0.6]$  in the following.

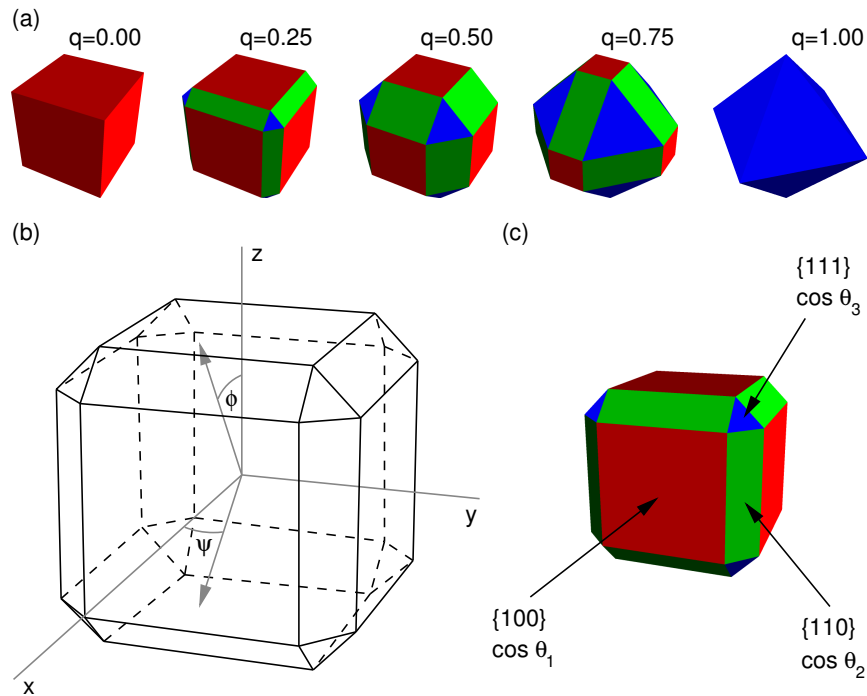


FIG. 1. (a) The truncated cube model for several values of the truncation parameter  $q \in [0, 1]$ . (b) A schematic representation of the model for  $q = 0.30$  which shows the truncated cube in its initial configuration, i.e., the normals of the  $\{100\}$  facets are axis-aligned and its centre coincides with the origin. We also indicated the azimuthal angle  $\psi$  and the polar angle  $\phi$ . To keep the picture clear, we did not show the interface or the height  $z$ , which is zero in this case. (c) The three types of facets: (red) a  $\{100\}$  facet, (green) a  $\{110\}$  facet, and (blue) a  $\{111\}$  facet. The figure also shows the corresponding cosine of the contact angle  $\cos \theta_i$ , with  $i = 1, 2, 3$ , that is used to describe the surface properties of the respective facets.

In its initial configuration the truncated cube has the normals of its  $\{100\}$  facets aligned with the axes of a standard Cartesian coordinate frame and its centre coincides with the origin. When this truncated cube is brought into contact

with a flat *undeformed* liquid-gas or liquid-liquid interface, the system can be described by four parameters: (i) the size of the particle, which is given by the multiplicative factor  $s$  that acts on the vertices in Eq. (1); (ii) the height  $z$  of the particle with respect to the interface (as measured along the  $z$ -axis), which we locate at  $z = 0$  ( $xy$ -plane); (iii) rotation by the azimuthal angle  $\psi$  (around the  $z$ -axis); and (iv) rotation by the polar angle  $\phi$  (around the  $y$ -axis). The angles are indicated in Fig. 1b. We assume that the truncated cube is first scaled by  $s$ , then rotated by  $\psi$  and subsequently by  $\phi$ , and finally it is translated by  $z$ . Due to the symmetry properties of the truncated cube we can restrict ourselves to  $\psi \in [0, \pi/4]$  and  $\phi \in [0, \pi/2]$ . Even for this restricted range there are several instances of duplicate orientations, e.g.,  $\psi \in [0, \pi/4]$  and  $\phi = 0$  gives essentially the same configuration as  $\psi = 0$  and  $\phi = \pi/2$ . These duplicate configurations are taken into account via congruence in our analysis.

### The Free Energy of Adsorption

In the experiments there is an indication that the surface properties of the different facets can vary with the particle concentration, see the main text. Effectively, the ligand covering of the various facets is influenced by the ligand concentration in the ethylene glycol via adsorption-desorption equilibria. To describe this in our model, we assume that the different crystal planes, i.e., the  $\{100\}$ ,  $\{110\}$ , and  $\{111\}$  facets, have surface properties that can vary independently of each other, but are otherwise the same for facets of the same type. In this system the free energy of adsorption  $F$  can be written as

$$F(z, \psi, \phi) = \gamma_{12}(A - S_{12}) + \gamma_{1t}S_{1t} + \gamma_{1b}S_{1b} + \gamma_{2t}S_{2t} + \gamma_{2b}S_{2b} + \gamma_{3t}S_{3t} + \gamma_{3b}S_{3b}, \quad (2)$$

where  $\gamma_{12}$  is the liquid-air interfacial tension,  $A$  is the total surface area of the interface,  $S_{12}$  is the surface area excluded from the interface by the presence of the colloid,  $\gamma_{it}$  is the surface tension between facets of type  $i$  ( $i = 1, 2, 3$ ) and the top medium,  $S_{it}$  is the total surface area of the facets of type  $i$  in contact with the top medium,  $\gamma_{ib}$  is the surface tension between facets of type  $i$  and the bottom medium, and  $S_{ib}$  is the total surface area of the facets of type  $i$  in contact with the bottom medium. Note that we have made the dependence of  $S_{12}$ ,  $S_{it}$ , and  $S_{ib}$  on  $(z, \psi, \phi)$  implicit. In this model the microscopic degrees of freedom of the solvent molecules were integrated out to give surface tensions. We further assumed that the interface is not deformed by the presence of the particle: capillary deformation by gravity, electrostatic effects, or contact-angle requirements. These are strong simplifications, but there are too many unknowns regarding the experimental system to justify a more extended model. In this light, the results obtained in the next section should be seen as an indication of the possible behaviour of a truncated cube at a liquid-air or liquid-liquid interface, rather than a full theoretical description of the phenomenology in the experimental system. We will come back to the quality of these results in the discussion.

To simplify the calculations we can reduce Eq. (2) by subtracting a constant contribution to the free energy of adsorption

$$F'(z, \psi, \phi) = F(z, \psi, \phi) - [\gamma_{12}A + \gamma_{1b}(S_{1t} + S_{1b}) + \gamma_{2b}(S_{2t} + S_{2b}) + \gamma_{3b}(S_{3t} + S_{3b})]; \quad (3)$$

$$= (\gamma_{1t} - \gamma_{1b})S_{1t} + (\gamma_{2t} - \gamma_{2b})S_{2t} + (\gamma_{3t} - \gamma_{3b})S_{3t} - \gamma_{12}S_{12}; \quad (4)$$

$$= \gamma_{12} [\cos \theta_1 S_{1t} + \cos \theta_2 S_{2t} + \cos \theta_3 S_{3t} - S_{12}], \quad (5)$$

where we set the shifted free energy  $F'$  to zero when the colloid is completely immersed in the bottom medium. In the last step [Eq. (5)] we used Young's equation [2]

$$\gamma_{it} = \gamma_{12} \cos \theta_i + \gamma_{ib}, \quad (6)$$

with  $\theta_i$  the contact angle corresponding to the (type  $i$  facet - top medium - bottom medium) three-phase contact. Figure 1c shows the correspondence between the different contact angles and the various facets: the surface properties of the  $\{100\}$  facets are described by  $\theta_1$ , those of  $\{110\}$  facets by  $\theta_2$ , and those of the  $\{111\}$  facets by  $\theta_3$ . Note that the  $\theta_i$  are determined by material properties, whereas  $\psi$  and  $\phi$  are variables in our theory. Using the above equations we can now write the dimensionless free energy of adsorption as

$$f(z, \psi, \phi) \equiv \frac{F'(z, \psi, \phi)}{\gamma_{12}S}; \quad (7)$$

$$= \cos \theta_1 r_{1t} + \cos \theta_2 r_{2t} + \cos \theta_3 r_{3t} - r_{12}, \quad (8)$$

with  $r_{it} \equiv S_{it}/S$  and  $r_{12} \equiv S_{12}/S$ . Note that the dependence of  $f$  on the level of truncation  $q$  and the surface properties and media (via the contact angles  $\theta_i$ ) is implicit in Eq. (7). Moreover, Eq. (7) is independent of the size  $s$  of the particle.

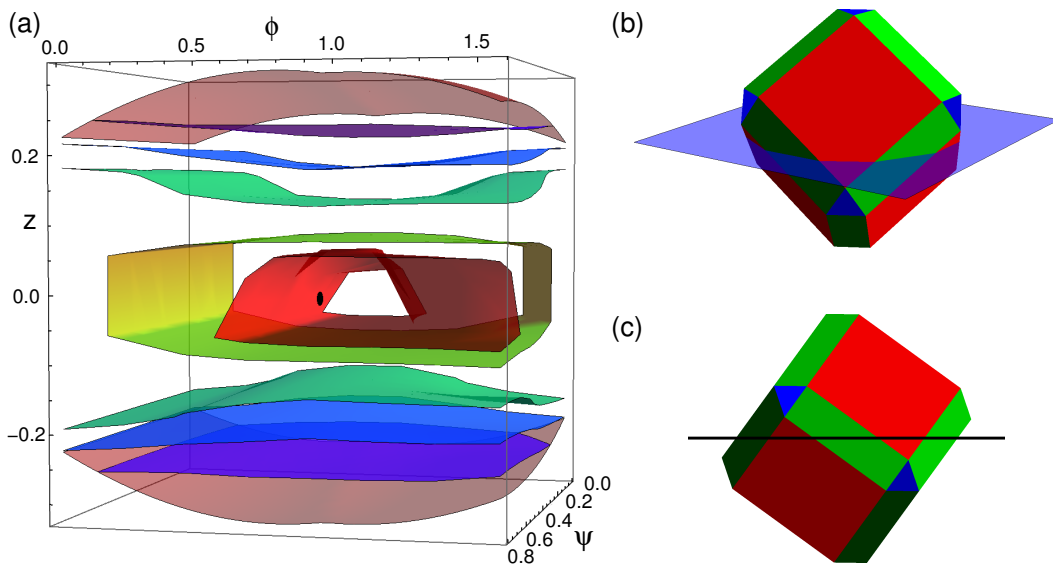


FIG. 2. The free energy of adsorption  $f$  for a truncated cube model with  $q = 0.30$  and  $\cos \theta_i = 0$ , for  $i = 1, 2, 3$ . Note that this choice for the contact angles ensures that adsorption is completely determined by excluded surface area considerations, also see Eq. (7). (a) A contour plot of the three-dimensional (3D) free-energy landscape:  $f$  as a function of the adsorption depth  $z$ , the azimuthal angle  $\psi$ , and the polar angle  $\phi$ . The top and bottom red surface indicate for which  $z$  value the truncated cube just touches the interface, for a given  $\psi$  and  $\phi$ . From blue to red the contours give  $f = -0.05, -0.10, -0.15, -0.20$ , and  $-0.22$ . The location of the free-energy minimum is indicated using a black dot. For this particular system we find that  $f(z, \psi, \phi)_{\min} \approx -0.24$  and that  $(z, \psi, \phi)_{\min} \approx (0.00, 0.25\pi, 0.30\pi)$ . (b) The truncated cube in its equilibrium position; one of the  $\{111\}$  facets is pointing in the direction of the  $z$ -axis. The translucent blue square indicates the interface. (c) A side view of the truncated cube in this equilibrium position, the thick black line indicates the interface.

For a given  $q$ ,  $\theta_1$ ,  $\theta_2$ , and  $\theta_3$ , Eq. (7) gives rise to a three-dimensional (3D) free energy of adsorption landscape, see Fig. 2 for an example. This landscape was established by numerically determining the values of  $r_{1t}$ ,  $r_{2t}$ ,  $r_{3t}$ , and  $r_{12}$  on a  $(z, \psi, \phi)$  grid, which can be easily accomplished using the triangular-tessellation technique described in Refs. [3, 4]. In the case of a faceted particle our technique's results are exact. The normalization in Eq. (1) allows us to directly obtain the fractional values  $r_{it}$  and  $r_{12}$ . In the following we take  $z \in [-0.4, 0.4]$ ,  $\psi \in [0, \pi/4]$ , and  $\phi \in [0, \pi/2]$  with 100 equidistant steps for each of these parameters. Whenever  $s = 1$ , the radius of a circumscribed sphere for our truncated cube is always smaller than 0.4. This implies that our choice of  $z \in [-0.4, 0.4]$  always samples the full range of adsorption configurations.

The thermodynamic equilibrium is assumed in the minimum of the free-energy landscape, i.e., the  $z$ ,  $\psi$ , and  $\phi$  combination for which  $f$  has the lowest value; we will denote this minimum as  $(z, \psi, \phi)_{\min}$ . This point can be easily approximated by searching through our free-energy landscape on a grid for the  $(z, \psi, \phi)$  combination that gives the lowest value of  $f$ . The density of grid points ( $100^3$ ) allows us to approach the actual minimum  $(z, \psi, \phi)_{\min}$  to within a sufficient level of precision to justify further analysis. Note that the presence of metastable minima in the free energy of adsorption is not taken into consideration by analysing the lowest free-energy value only.

### Results of our Theoretical Study

An advantage of our model is that the  $r_{it}$  and  $r_{12}$  only have to be determined only once for a given  $q$  in order to establish  $f(z, \psi, \phi)$  for different values of  $\theta_i$ . To probe the effect of different surface patterning on  $(z, \psi, \phi)_{\min}$ , or equivalently different ligand concentrations on the facets, we varied  $\cos \theta_i \in [-1, 1]$  in equidistant steps of 0.03.

Figure 3 shows the distribution of  $(z, \psi, \phi)_{\min}$  in the 3D  $(z, \psi, \phi)$  landscape upon varying the contact angles for  $q = 0.30$ . Note that the distribution of  $(z, \psi, \phi)_{\min}$  is not homogeneous. In fact, an analysis of our results shows that the equilibrium orientations of the truncated cube can be roughly divided into three categories: (i) the normal of one of the  $\{100\}$  facets is pointing in the direction of the  $z$ -axis, (ii) the normal of one of the  $\{110\}$  facets is pointing in the direction of the  $z$ -axis, and (iii) the normal of one of the  $\{111\}$  facets is pointing in the direction of the  $z$ -axis, also see Fig. 4. We refer to these three configurations as the 'prototypical' configurations. This rough division assumes

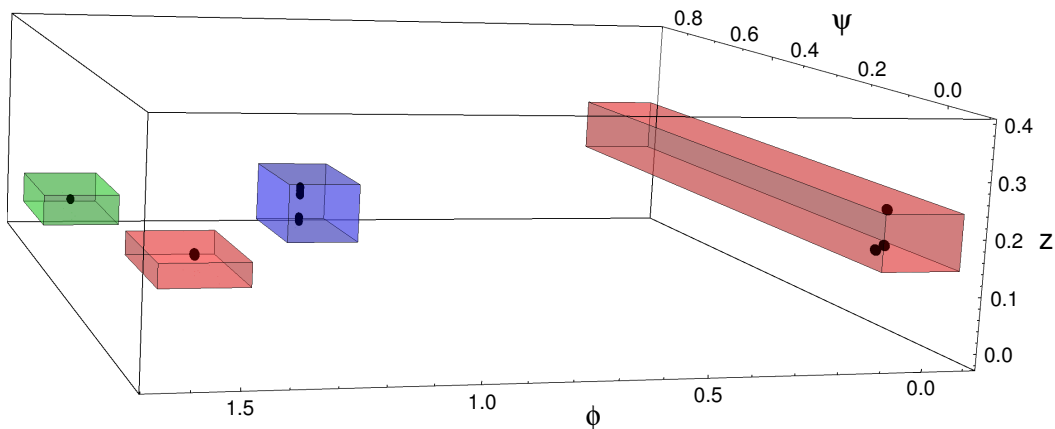


FIG. 3. The distribution of equilibrium adsorption configurations  $(z, \psi, \phi)_{\min}$  (black dots) obtained by varying  $\cos \theta_i \in [-1, 1]$  ( $i = 1, 2, 3$ ) in equidistant steps of 0.03 for a truncated cube with  $q = 0.30$ . Note that the distribution of  $(z, \psi, \phi)_{\min}$  is not homogeneous, only a few of the possible values of  $(z, \psi, \phi)$  are assumed. The red, green, and blue translucent boxes indicate to which ‘prototypical’ configuration we assign these  $(z, \psi, \phi)_{\min}$  points. Configurations in the red boxes correspond to adsorption with the normal of one of the  $\{100\}$  facets pointing in the direction of the  $z$ -axis, configurations in the green box correspond to adsorption with the normal of one of the  $\{110\}$  facets pointing in the direction of the  $z$ -axis, and configurations in the blue box correspond to the normal of one of the  $\{111\}$  facets pointing in the direction of the  $z$ -axis; also see Fig. 4, which uses the same colour coding. The two red boxes accommodate a single congruence class.

that, for instance, the state where the particle is adsorbed at depth  $z$  is equivalent to the one where it is adsorbed at depth  $-z$ . Moreover, we assume that  $|\psi' - \psi| < 0.03\pi$  and  $|\phi' - \phi| < 0.03\pi$  constitute the same configuration, where  $\psi'$  and  $\phi'$  are the angles corresponding to the prototypical orientation of one of the three categories. The tolerance in the depth  $z$  is considered on a case-by-case basis.

Working backwards we can now find the three values of  $\cos \theta_i$  for which the truncated cube is in one of the prototypical equilibrium configurations, see Fig. 4, which shows this correspondence. Here we only give  $\cos \theta_1, \cos \theta_2 \in [-1, 1]$  and  $\cos \theta_3 \in [0, 1]$ , since the graph is point symmetric in the origin, which can be easily shown by considering the signs of the cos terms in Eq. (7). We find that the  $\{100\}$ -prototypical equilibrium configuration is the most common and there is a slightly greater number of  $\{111\}$  than  $\{110\}$  equilibrium configurations. However, it should be noted that interpreting the graph on the basis of surface area alone can be misleading, since  $\theta_i \gtrsim 150^\circ$  and  $\theta_i \lesssim 30^\circ$  represent atypical values of the contact values, i.e.,  $|\cos \theta| \lesssim 0.87$  is reasonable.

Following the approach that we employed for  $q = 0.30$ , we can study the influence of the surface properties of the different types of facet as a function of the level of truncation  $q$ , also see Figs. 5 - 8. Note that for  $q = 0$  there are only two types of equilibrium configuration, one where one of the  $\{100\}$  facets is pointing upward, and one where one of the ‘ $\{110\}$  facets’ is pointing upward. The first can be explained by the particle minimizing its contact area with the unfavoured medium, whilst still excluding a piece of the interface (thereby lowering its free energy). The second arises when there is a limited difference between the two media; the colloid can lower the free energy by excluding the maximum amount of surface area from the interface. N.B., for a cube ( $q = 0$ ) the two prototypical configurations are the *only* two possible configurations within the confines of our model, i.e., there is no spread in the  $(z, \psi, \phi)_{\min}$ .

For small levels of truncation  $q = 0.15$ , see Fig. 6, the division into two prototypical equilibrium configurations ( $\{100\}$  and  $\{110\}$ ) remains. The spread of the  $(z, \psi, \phi)_{\min}$  around these configurations increases. The surface properties of the  $\{110\}$  facets have a small influence on the configurations that are assumed by the truncated cubes, as can be seen in Fig. 6. However, the presence of  $\{111\}$  facets do not seem to affect the equilibrium configurations sufficiently to cause the third prototypical configuration to appear.

Further truncation of the cube, see Fig. 4 for the  $q = 0.30$  and Fig. 7 for the  $q = 0.45$  result, respectively, appears to promote the  $\{111\}$  prototypical configuration. It is likely that a greater level of truncation destabilizes the  $\{110\}$  configuration in favour of the  $\{111\}$  configuration, because the maximum amount of surface area that can be excluded from the interface in either configuration becomes comparable. This hypothesis was confirmed by considering truncated cubes with homogeneous surface properties, as well as other ways of truncating a cube [5].

However, when the level of truncation is great, see Fig. 8 for the  $q = 0.60$  result, the truncated cube becomes rather spherical. This implies that there is no longer a limited number of favoured orientations on the basis of excluded

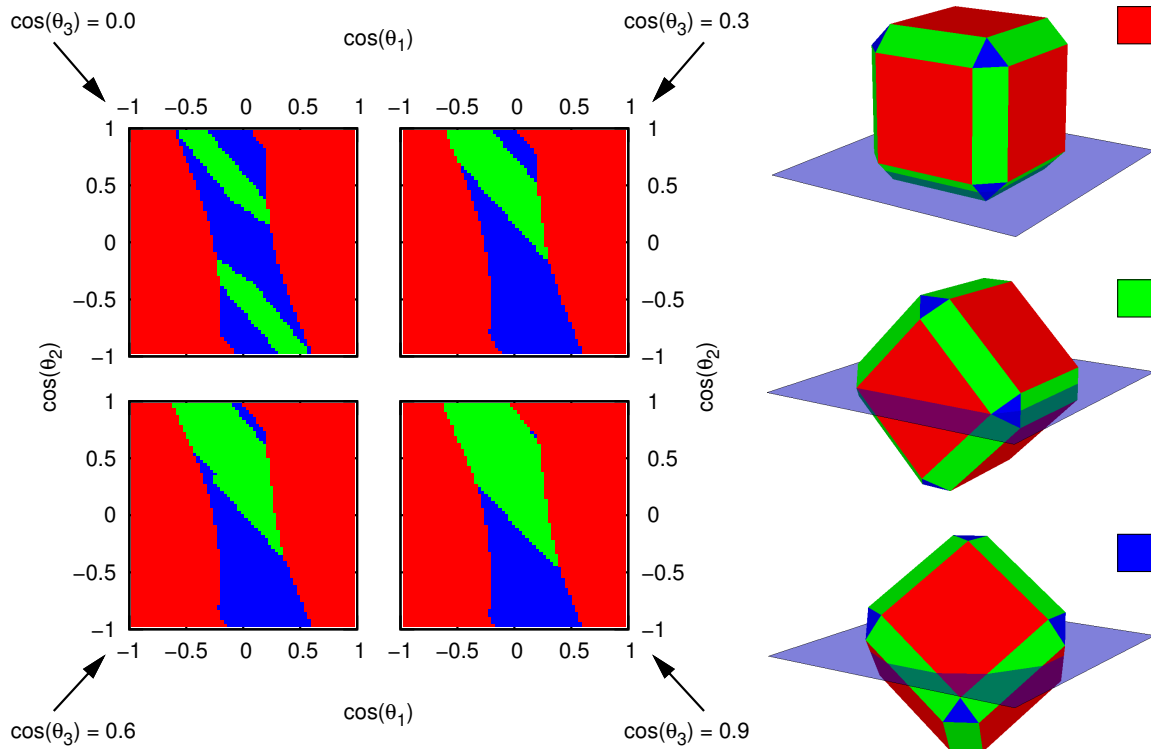


FIG. 4. The equilibrium configurations that present themselves for a truncated cube with truncation level  $q = 0.30$  as a function of its surface properties. The sub-plots show four  $\cos \theta_3$  slices: top,  $\cos \theta_3 = 0.0$  (left) and  $\cos \theta_3 = 0.3$  (right); bottom,  $\cos \theta_3 = 0.6$  (left) and  $\cos \theta_3 = 0.9$  (right). These indicate the prototypical equilibrium configuration that is assumed by the truncated cube as a function of  $\cos \theta_1$  and  $\cos \theta_2$ . (legend) The three equilibrium configurations and associated colour code: (red) the normal of one of the  $\{100\}$  facets is pointing in the direction of the  $z$ -axis, (green) the normal of one of the  $\{110\}$  facets is pointing in the direction of the  $z$ -axis, and (blue) the normal of one of the  $\{111\}$  facets is pointing in the direction of the  $z$ -axis.

surface area arguments. As can be appreciated from Fig. 8 this results in a more coarse distribution of ‘prototypical’ equilibrium configurations, as well as the appearance of three more configurations.

### Discussion and Outlook

Let us first consider the likelihood of interfacial adsorption. For a spherical particle with homogeneous surface properties the minimum difference in free energy  $\Delta F$  between the adsorbed and desorbed state is easily shown to be given by  $\Delta F = \pi a^2 \gamma_{12} (1 - |\cos \theta|)^2$ . Here,  $a$  is the radius of the sphere,  $\theta$  is the (air/liquid)-sphere-liquid contact angle, and  $\gamma_{12}$  is the interfacial surface tension. We can use this value to estimate what the strength of adsorption for our nanocrystals might be.

We assume that the nanocrystals are at the air/toluene interface, based on previous experimental observations for similar systems [6, 7]. The surface tension of the air/toluene interface is given by  $\gamma_{12} \approx 2.8 \cdot 10^{-2} \text{ Nm}^{-1}$  [8]. Note that finite values of  $\cos \theta$  lower  $\Delta F$ . However, for realistic values of  $\theta$  this reduction in  $\Delta F$  is no more than a factor of 10, with the maximum in  $\Delta F$  assumed when  $\cos \theta = 0$ . The smaller nanocrystals, which have a diameter of 5.4 nm, therefore adsorb to the interface with at most  $\Delta F \approx 1 \cdot 10^2 \text{ k}_B\text{T}$ , where  $\text{k}_B$  is Boltzmann’s constant and  $T$  is the temperature. The larger nanocrystals, which have diameter of 9.9 nm, adsorb with at most  $\Delta F \approx 5 \cdot 10^2 \text{ k}_B\text{T}$ . This *simple* estimate gives some ab initio justification of the applicability of our theoretical results to the experimental system. Under ideal circumstances there will be a strong influence of the interface on the nanoparticles, which drives these towards their equilibrium adsorption configuration. It should, however, be mentioned that these estimates do not factor into account surface-tension lowering effects such as the presence of surfactants at the interface or pollutants in the toluene.

Our results indicate that the three experimentally observed configurations can be explained within the framework of

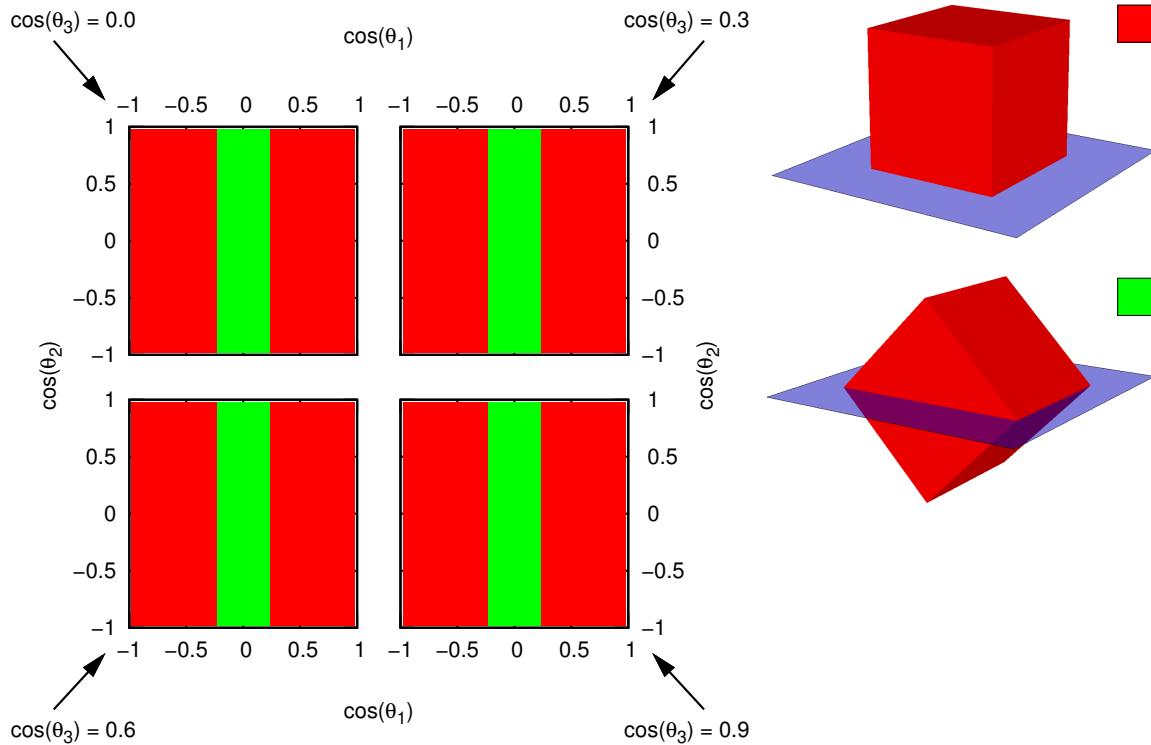


FIG. 5. The equilibrium configurations that present themselves for a cube ( $q = 0$ ) as a function of its surface properties. The sub-plots indicate the (prototypical) equilibrium configuration that is assumed by the cube as a function of  $\cos \theta_1$  and  $\cos \theta_2$ , for various  $\cos \theta_3$  values. (legend) The two equilibrium configurations and associated colour code. Note that the type of configuration only depends on the surface properties of the red  $\{100\}$  facets, as expected for this level of truncation.

adsorption-desorption equilibria for the ligand concentration on the various facets. Indeed, upon varying the surface properties of the three types of facet - by modifying the contact angle - we theoretically found the possible equilibrium adsorption configurations to coincide with the orientations of the particles in the superstructures that formed at the interface. Moreover, it was experimentally observed that the level of truncation for the larger nanocrystals (9.9 nm) was less than that for the smaller variety (5.4 nm). This could explain the fact that the honeycomb structures were only observed for the smaller nanocrystals, since the  $\{111\}$  adsorption configuration does not occur for smaller levels of truncation, within the confines of our model.

We therefore propose the following explanation for our observations. At low concentrations of the truncated cubes the adsorption-desorption equilibrium for the ligands covering the facets is shifted towards the ligands being preferentially adsorbed in the ethylene glycol. When the truncated particles come together there is irreversible and disordered aggregation. However, for higher particle concentrations the equilibrium shifts to a sufficiently high ligand covering of the facets that immediate aggregation is prevented. Moreover, we believe that for these systems the surface properties of the nanoparticles are such that the equilibrium adsorption configuration is of the  $\{100\}$  or the  $\{110\}$  type, where the latter is preferentially assumed for lower particle concentrations. These configurations lead to the formation of two-dimensional (2D) rod-like ( $\{110\}$ ) and square assemblies ( $\{100\}$ ) by oriented attachment via the  $\{100\}$  facets, respectively. That is to say, for the  $\{100\}$ -like configuration, four of the  $\{100\}$  facets are oriented perpendicular to the interface, allowing for oriented attachment via these facets in the plane of the interface, which gives rise to square structures. For the  $\{110\}$  configuration, only two (opposing)  $\{100\}$  facets are perpendicular to the interface, allowing for oriented attachment that results in linear structures. Upon increasing the nanoparticle concentration from low to intermediate values, the ligand adsorption/desorption equilibria are shifted resulting in a different nanoparticle surface pattern. This surface pattern leads to preferential adsorption at the interface of the  $\{111\}$  type and subsequent oriented attachment via the (now) exposed  $\{110\}$  facets of the particles into honey-comb superstructures. The latter situation does not, however, occur when the level of truncation is too small to allow for the  $\{111\}$  configuration to be stable.

It is important to note that our results (and the conclusions we based on these) were obtained using a *simple* model

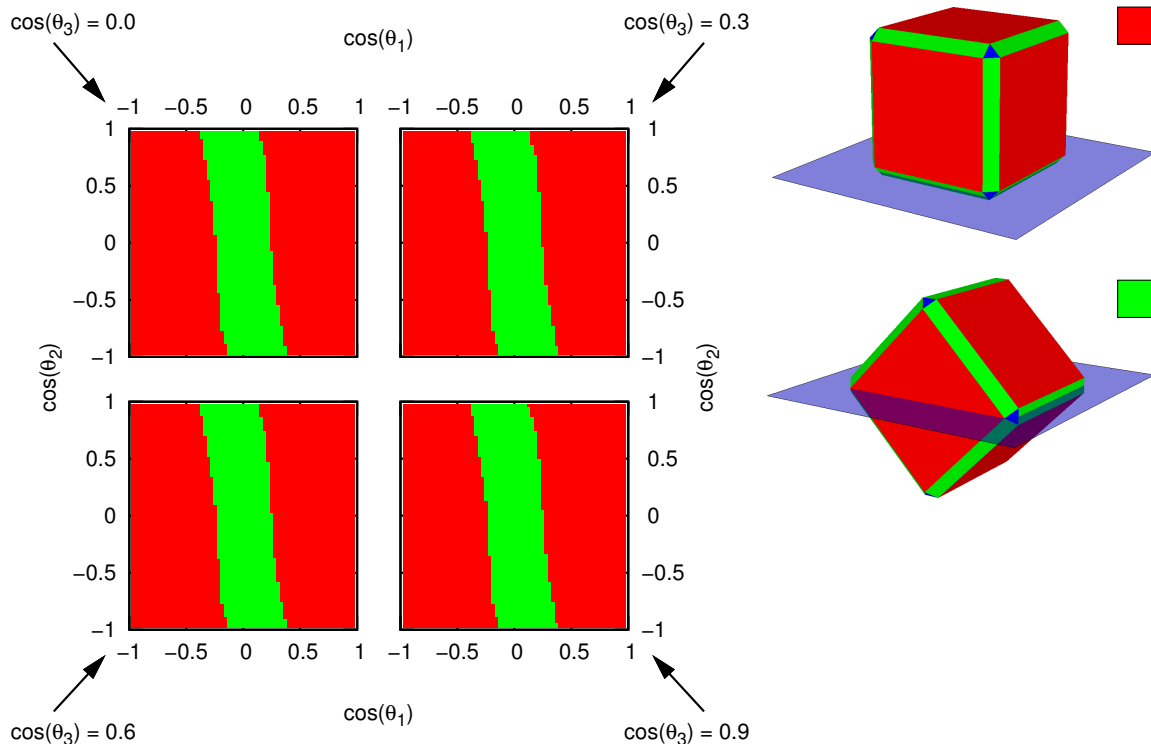


FIG. 6. The equilibrium configurations that present themselves for a truncated cube with truncation level  $q = 0.15$  as a function of its surface properties. The sub-plots indicate the (prototypical) equilibrium configuration that is assumed by the truncated cube as a function of  $\cos \theta_1$  and  $\cos \theta_2$ , for various  $\cos \theta_3$  values. (legend) The two equilibrium configurations and associated colour code. Note that there is a small dependence on the surface properties of the  $\{110\}$  facets ( $\cos \theta_2$ ) for this level of truncation. However, the surface properties of the  $\{111\}$  facets do not appear to play a role.

for the adsorption of a particle at a liquid-liquid or liquid-air interface. We leave a full investigation of the experimental phenomenology by theoretical or simulation means as an open problem for future study. An interesting question for such a study to answer is if a simple model that incorporates particle-concentration-based ligand adsorption-desorption equilibria, is capable of capturing the shift from the  $\{100\}$  towards the  $\{111\}$  equilibrium configuration, whilst at the same time showing a lower ligand covering of the facets which we believe to mediate the oriented attachment. A conformation of this shift would give strong support for our hypothesis that the interface and ligand adsorption/desorption play a crucial role in determining the structure of the assemblies that we observed to form by oriented attachment.

\* D.vanmaekelbergh@uu.nl

- [1] P. Pieranski, Phys. Rev. Lett. **45**, 569 (1980).
- [2] T. Young, Phil. Trans. R. Soc. Lond. **95**, 65 (1805).
- [3] J. de Graaf, M. Dijkstra, and R. van Roij, Phys. Rev. E **80**, 051405 (2009).
- [4] J. de Graaf, M. Dijkstra, and R. van Roij, J. Chem. Phys. **132**, 164902 (2010).
- [5] J. de Graaf, *Anisotropic nanocolloids: Self-Assembly, Interfacial Adsorption, and Electrostatic Screening*, PhD thesis, Utrecht University, 2012, ISBN 978-90-393-5797-2.
- [6] H. Friedrich et al., Nano Lett. **9**, 2719 (2009).
- [7] D. K. Smith, B. Goodfellow, D.-M. Smilgies, and B. A. Korgel, J. Am. Chem. Soc. **131**, 3281 (2009).
- [8] A. W. Adamson and A. P. Gast, *Physical Chemistry of Surfaces*, Wiley-Interscience (New York), 6th edition, 1997.

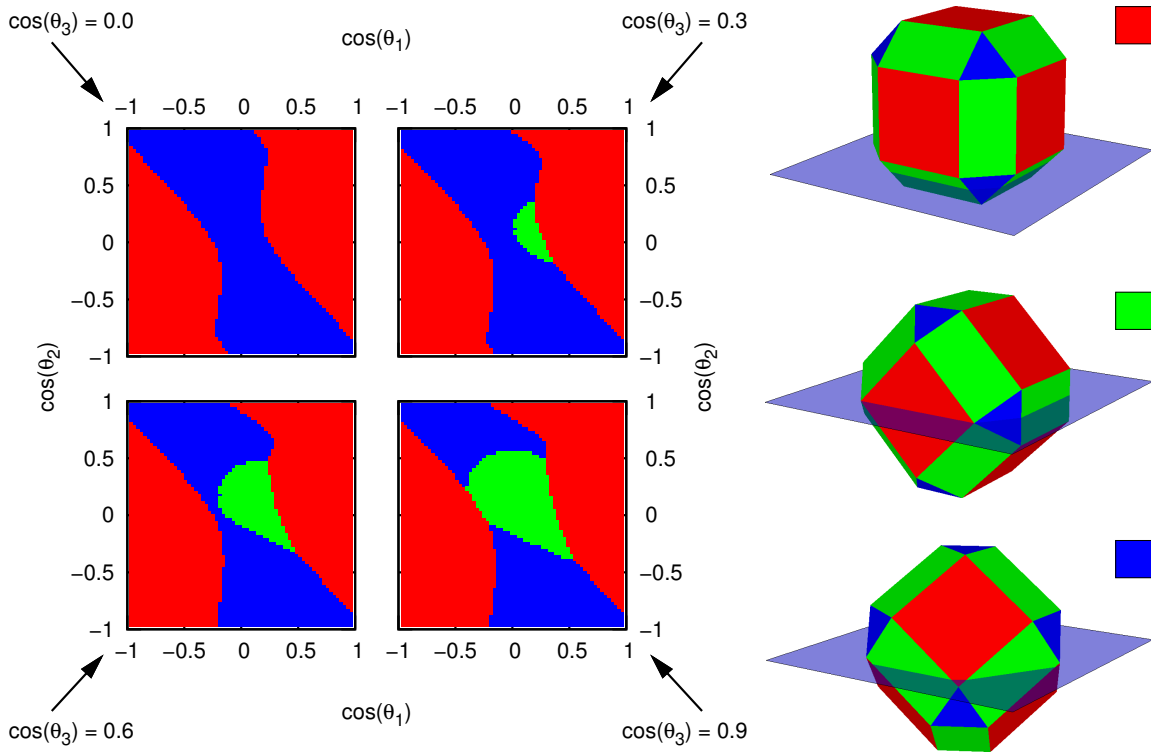


FIG. 7. The equilibrium configurations that present themselves for a truncated cube with truncation level  $q = 0.45$  as a function of its surface properties. The sub-plots indicate the prototypical equilibrium configuration that is assumed by the truncated cube as a function of  $\cos \theta_1$  and  $\cos \theta_2$ , for various  $\cos \theta_3$  values. (legend) The three equilibrium configurations and associated colour code.

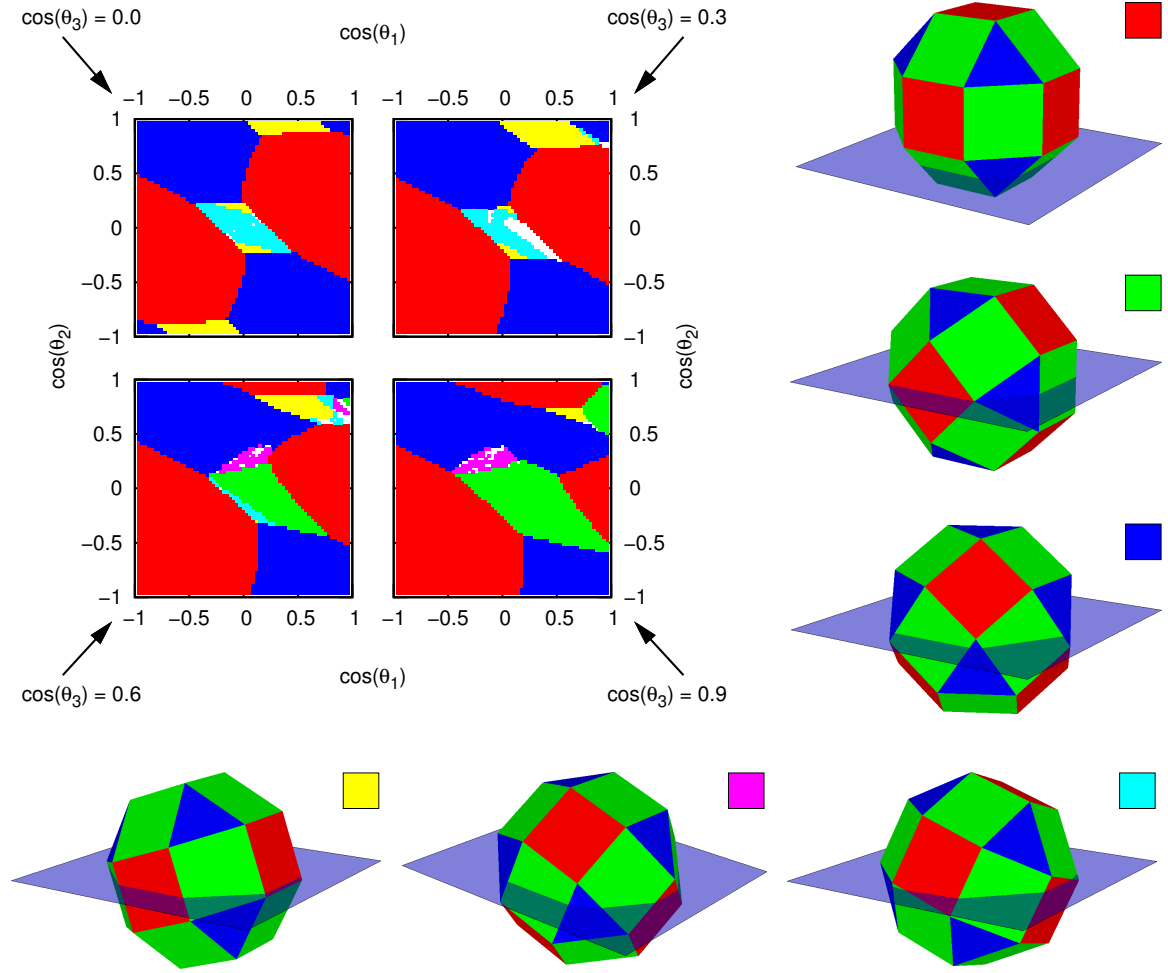


FIG. 8. The equilibrium configurations that present themselves for a truncated cube with truncation level  $q = 0.60$  as a function of its surface properties. The sub-plots indicate the prototypical equilibrium configuration that is assumed by the truncated cube as a function of  $\cos\theta_1$  and  $\cos\theta_2$ , for various  $\cos\theta_3$  values. (legend) The six prototypical equilibrium configurations and associated colour codes. (red) one of the  $\{100\}$  facets is pointing in the direction of the  $z$ -axis, (green) one of the  $\{110\}$  facets is pointing in the direction of the  $z$ -axis, (blue) one of the  $\{111\}$  facets is pointing in the direction of the  $z$ -axis, (yellow) the  $\{210\}$  'facet' is pointing in the direction of the  $z$ -axis, (magenta) the  $\{221\}$  'facet' is pointing in the direction of the  $z$ -axis, and (cyan) the  $\{321\}$  'facet' is pointing in the direction of the  $z$ -axis. The white points in the sub-plots indicate for which  $\cos\theta_i$  combinations we were unable to assign a prototypical equilibrium configuration.